

1 **Optical coherence tomography: history, current status and laboratory work**

2

3 **Authors:** Michelle L Gabriele,^{1,2,3} Gadi Wollstein,¹ Hiroshi Ishikawa,^{1,2} Larry Kagemann,^{1,2}

4 Juan Xu,¹ Lindsey S Folio,¹ Joel S. Schuman^{1,2,3,4}

5

6 **Affiliations:** ¹Department of Ophthalmology, UPMC Eye Center, Eye and Ear Institute,

7 Ophthalmology and Visual Science Research Center, University of Pittsburgh School of

8 Medicine, Pittsburgh, PA; ²Department of Bioengineering, Swanson School of Engineering,

9 University of Pittsburgh, Pittsburgh, PA; ³Center for the Neural Basis of Cognition, University of

10 Pittsburgh and Carnegie Mellon University, Pittsburgh, PA; ⁴McGowan Institute for

11 Regenerative Medicine, University of Pittsburgh, Pittsburgh, PA

12

13 **Financial Support:** Supported in part by National Institute of Health grants R01-EY13178, and

14 P30-EY08098 (Bethesda, MD), The Eye and Ear Foundation (Pittsburgh, PA) and an

15 unrestricted grant from Research to Prevent Blindness (New York, NY).

16

17 **Conflict of Interest Disclosures:** Dr. Wollstein received research funding from Carl Zeiss

18 Meditec and Optovue. Drs. Wollstein, Ishikawa, Xu and Schuman have intellectual property

19 licensed by the University of Pittsburgh to Bioptigen. Dr. Schuman received royalties for

20 intellectual property licensed by Massachusetts Institute of Technology to Carl Zeiss Meditec.

21

- 1 **Corresponding Author:** Joel Schuman, MD, UPMC Eye Center, Department of
- 2 Ophthalmology, University of Pittsburgh School of Medicine, 203 Lothrop Street, Eye and Ear
- 3 Institute, Suite 816, Pittsburgh, PA 15213, Tel: 412-647-2205, E-mail: schumanjs@upmc.edu.

1 **Abstract**

2

3 Optical coherence tomography (OCT) imaging has become widespread in ophthalmology over
4 the past 15 years due to its ability to visualize ocular structures at high resolution. This article
5 reviews the history of OCT imaging of the eye, current status and laboratory work that is driving
6 the future of the technology.

1 **A Brief History of Optical Coherence Tomography in Ophthalmology**

2 Optical coherence tomography (OCT) has advanced considerably since it was first applied to the
3 eye.¹⁻⁷ OCT is an extension of a technique called low-coherence interferometry, which was
4 initially applied to ophthalmology for *in-vivo* measurements of eye axial length.¹ At the time of
5 introduction, OCT was used to obtain *in-vivo* optical cross-sections of the anterior segment⁶ as
6 well as retinal pathologies such as macular detachment, macular hole, epiretinal membrane,
7 macular edema and idiopathic central serous chorioretinopathy.⁴ OCT cross-sections were also
8 used to evaluate the optic disc and retinal layers^{5, 8} such as the retinal nerve fiber layer (RNFL).⁹
9 Scan patterns that enabled reproducible measurements were developed¹⁰ and these eventually
10 became incorporated into a commercial system, which had an axial resolution of $\sim 10\mu\text{m}$.

11
12 The first clinical system was limited to a scanning speed of 400 axial-scans (A-scans)/second due
13 to a physical constraint: a moving reference mirror. OCT uses low coherence interferometry to
14 obtain A-scan intensity profiles, and this requires light to be split and sent to both a reference
15 arm with a mirror and to the sample. Provided the path length to the reference mirror and tissue
16 match to within the coherence length of the light source, when the reflected beams recombine,
17 interference occurs. Intensity information, in the form of a reflectivity profile in depth, can be
18 extracted from the interference profile. Changing the location of the reference mirror allows
19 backscattered tissue intensity levels to be detected from different depths in the tissue sample.
20 This approach is referred to as time-domain (TD)-OCT because time-encoded signals are
21 obtained directly. Several improvements in OCT hardware have been introduced since the first
22 commercial TD-OCT system became available. Better axial resolution¹¹⁻¹³ and increased

1 scanning speed¹⁴⁻²³ are the two main advancements that have recently become incorporated into
2 commercial systems.

3

4 The implementation of broad-band light sources into OCT systems¹¹ improved the axial
5 resolution from $\sim 10\mu\text{m}$ to as high as $2\mu\text{m}$ in tissue.²⁴ Acquisition speed has improved
6 considerably by detecting backscattering signals in the frequency domain,¹⁴⁻²³ which means
7 backscattered depth information at a given location can be collected without the movement of a
8 reference mirror. Frequency information is acquired using either a broad bandwidth light source,
9 charge-coupled device (CCD) camera and spectrometer,^{14, 17, 18, 20} or by sweeping a narrow
10 bandwidth source through a broad range of frequencies and using a photodetector.^{16, 21-23} The
11 approach using a broadband light source is often referred to as spectral domain (SD)-OCT, while
12 the latter is termed swept-source (SS)-OCT. In both approaches, intensity profiles (A-scans) are
13 obtained using a Fourier-transform of the detected frequencies, and this facilitates rapid A-scan
14 collection. In addition to improved scanning speed, frequency-domain OCT also offers the
15 advantage of higher detection sensitivity, i.e., it will exhibit higher signal-to-noise given a
16 perfect reflector.^{23, 25} A summary of OCT detection techniques can be seen in Table 1.

17

18 With these speed and sensitivity improvements, it is now feasible to collect volumetric (three-
19 dimensional; 3D) scans of tissue whereas in the past, the amount of time required to do this
20 would have been prohibitive. Broadband volumetric retinal imaging with SD-OCT at speeds of
21 up to 312,500 A-scans/sec²⁶ and SS-OCT 249,000 A-scans/sec²⁷ have been demonstrated. To
22 date, most clinical systems operate at an acquisition rate of $\sim 27,000$ A-scans/sec and an axial

- 1 resolution of 5-6 μm . A summary of the currently commercially available retinal imaging
- 2 systems is presented in Table 2.

1 **Current Status of Optical Coherence Tomography in the Clinic**

2

3 **Glaucoma**

4 Conventionally, the most common scan patterns in TD-OCT glaucoma imaging were a 3.4 mm
5 scan around the optic nerve head (ONH), and six equally spaced radial scans through the macula
6 (6 mm) and optic nerve (4 mm). RNFL thickness is obtained via automated RNFL segmentation
7 in the circumpapillary scan protocol, while macular thickness (internal limiting membrane, ILM,
8 to the photoreceptor inner segment-outer segment junction (IS-OS)) is automatically segmented
9 in the macular scan pattern. The optic nerve scan is used to obtain cup area, disc area, cup
10 diameter, disc diameter and rim area. These ONH parameters are obtained automatically: the
11 software detects the ONH margin/RPE tips, but the user can modify the location if the ONH
12 margin detection algorithm is inaccurate.

13

14 The ONH and RNFL scan protocols have been used since TD-OCT became commercially
15 available, and RNFL and ONH parameters have been shown to differ between glaucomatous and
16 healthy eyes.^{9, 28-33} Glaucoma discriminating ability, measured by the area under receiver
17 operating characteristic curves (AROC) of RNFL (AROC = 0.94) and disc parameters (eg, rim
18 area AROC= 0.97) have been reported to be higher than macular volume and thickness (AROC
19 both 0.80).³⁴ A similar glaucoma discriminating ability is seen in comparing TD-OCT imaging
20 and SD-OCT imaging when similar parameters are examined.³⁵ However, it may be possible to
21 further improve glaucoma discrimination using parameters obtained from 3D scanning. With the
22 commercialization of rapidly scanning SD-OCT systems, 3D volumes of tissue are now easily
23 acquired. A 3D dataset not only allows a quantitative analysis from more locations but, once a

1 volume has been collected, OCT fundus (*en face*) images can be obtained by integrating A-
2 scans.²⁰ These can be used for a subjective assessment of signal quality and to assist with
3 evaluating and/or correcting eye motion that may have occurred throughout the scan. The OCT
4 fundus image also allows registration of OCT cross-sections to precise retinal locations.

5
6 Acquisition of 3D datasets has led to the advancement of software methods for efficiently
7 analyzing and summarizing these vast amounts of data. One method for obtaining RNFL
8 thickness measurements has been sampling the 3D volume (eg, 6.0 x 6.0 x 2.0 mm, centered on
9 the ONH) after acquisition, at a diameter of 3.4 mm centered on the ONH (Figure 1). This
10 method has been shown to have higher reproducibility than the conventional TD-OCT 3.4 mm
11 scan circle, where the image is acquired along the circle only.³⁶ One explanation for the
12 improved performance is that, with TD-OCT, scan placement is dependent upon the user and can
13 be variable, but with SD-OCT, the circle can be consistently placed in the same location using
14 landmarks within the 3D volume.

15
16 While sampling 3D volumes after acquisition may be an effective way for summarizing RNFL
17 measurements, it is doing so at a cost: data outside the 3.4 mm band are not being used.
18 Subjectively, wedge defects and global thinning may be easy to spot, but subtle changes or
19 deviations from normal outside the 3.4 mm sampling band may be missed. One way of
20 addressing this is to create an RNFL thickness map, which consists of all thickness
21 measurements outside of the ONH. From this, thickness measurements from one subject can be
22 compared to population thickness measurements. To date, however, commercial software is

1 available for looking at deviation from normal, but there is no quantitative assessment utilizing
2 all of the available RNFL information.

3

4 Different approaches have been proposed for quantifying 3D data. 3D RNFL thickness was
5 analyzed in terms of a thickness profile as distance from the ONH increased.³⁷ In healthy eyes,
6 the slope of RNFL thickness increased near the margin of the ONH, peaked, and then decreased
7 with increasing distance from the ONH center in all but the nasal quadrant, which linearly
8 decreased starting from the disc margin. Another approach (Ishikawa H, et al. IOVS
9 2009;50:ARVO E-Abstract 3328) exploits 3D macular data, which have been summarized using
10 segmentation of the inner retinal complex (IRC: retinal ganglion cell layer (RGC), inner
11 plexiform layer (IPL), inner nuclear layer (INL); Figure 2).³⁸ This approach reduces IRC data to
12 superpixels (4x4 adjacent sampling points) and compares these superpixels to a normative
13 thickness superpixel dataset. By condensing measurements into superpixels, it is less likely that
14 small imaging artifacts or algorithm failure will have an effect.

15

16 One commercially available system has developed an approach for summarizing macular data
17 called the Ganglion Cell Complex (GCC; RTVue, Optovue, Inc) which consists of essentially the
18 same layers as the IRC: the RGC (retinal ganglion cell bodies), RNFL (RGC axons) and IPL
19 (RGC dendrites). The GCC measurements are then directly compared to a normative database
20 and thickness difference and significance maps are available (Figure 3).

21

22 While a comparison to a normal population may reveal differences, structural changes may be
23 occurring while a patient remains within normal limits and therefore go undetected. Ideally, a

1 longitudinal comparison could be made for a given individual to look for subtle structural
2 changes attributed to disease progression. One approach has been proposed by Kim *et al* to allow
3 compatibility between TD-OCT and 3D OCT device iterations.³⁹ Since TD-OCT devices have
4 been commercially available longer than 3D imaging systems, years of patient information may
5 be available. The method presented by Kim *et al* resamples a 3D-OCT dataset for every possible
6 3.4-mm circular scan location within the boundaries of the 3D-OCT volume. It then uses cross
7 correlation between these virtual circular scans and the TD-OCT 3.4-mm scan to automatically
8 match the TD-OCT scan circle location within the volume.

9
10 To longitudinally compare 3D volumes, however, image registration techniques must be
11 developed to spatially align 3D scans before they can be compared. This may be accomplished
12 using cross-correlation,^{40, 41} or by using landmarks within the OCT fundus image, such as blood
13 vessels.^{42, 43} Eye motion during acquisition has been shown to alter scan location,⁴⁴⁻⁴⁶ and the
14 effect of eye motion is visible on OCT *en face* images as discontinuous blood vessels. Detecting
15 and correcting blood vessel location to align the OCT fundus can help correct eye motion,⁴²
16 which may be useful for cross-sectional analysis.

17
18 Longer wavelength imaging ($\sim 1\mu\text{m}$ center wavelength) of the lamina cribrosa²⁷ and
19 birefringence imaging of the RNFL using polarization-sensitive (PS)-OCT⁴⁷⁻⁴⁹ are two
20 techniques under development that may improve the diagnosis and monitoring of glaucoma.
21 These are further described in the Pre-clinical and Laboratory Studies section of this review.

22
23 **Retina**

1 The macular scan pattern discussed above – 6 radial macular scans, 6 mm long, spaced 30° apart
2 – has traditionally been used in TD-OCT imaging to assess retinal parameters such as total
3 retinal thickness and the IRC. Three-dimensional imaging, however, has revolutionized the
4 examination of retinal pathologies.⁵⁰⁻⁵⁵ By examining the 3D structure of the retina, as opposed
5 to just six radial scans, subtle structural changes may become apparent. For example, using
6 high-resolution 3D imaging to observe the photoreceptor inner segment/outer segment junctions
7 may be an indicator of visual outcomes after macular hole surgery.⁵⁶⁻⁵⁸

8
9 At present, one application of 3D OCT of imaging retinal pathologies that has considerable
10 clinical potential is surgical planning and the evaluation of surgical outcomes. The use of OCT
11 for planning an access point to release the hyaloid for vitrectomy using the six radial scan pattern
12 in TD-OCT has been described.⁵⁹ While this was effective for minimizing traction forces on the
13 macula during surgery, a detailed 3D map of the hyaloid membrane and subhyaloid space could
14 further inform the clinician. Falker-Radler et al have used 3D imaging to visualize the
15 vitreomacular interface in subjects that were undergoing surgery for epiretinal membrane.⁶⁰
16 Others have used OCT for evaluation of structure after surgery for macular hole^{57, 58, 61} and
17 vitreomacular traction.^{52, 62-64} The use of 3D imaging for surgical preparation and evaluation of
18 surgical outcomes has the potential to improve with the use of longer wavelength imaging, which
19 is described later in this review. Automated segmentation of structures of interest, when possible,
20 may provide objective measurements to clinicians for pre- and post-surgical evaluation.
21
22 Quantification of thickness is possible in certain pathologies,^{65, 66} especially with early stage
23 changes.^{67, 68} The reproducibility of SD-OCT retinal thickness measurements is higher in than

1 that of TD-OCT.⁶⁹ Thickness has been shown to correlate with best-corrected visual acuity in
2 diabetic macular edema⁷⁰ and ERM.⁷¹ While thickness may be a clinically useful correlate of
3 visual function, however, there are cases and pathologies where no correlation to thickness is
4 seen and thus clinicians need to exercise caution in interpretation of thickness measurements.⁷²

5
6 Drusen volume may be a predictor of progression of age-related macular degeneration,⁶⁵ and
7 efforts are underway for automated assessment.⁶⁶ While accurate quantification of volumetric
8 tissue changes will assist with longitudinal monitoring of disease, fully automated segmentation
9 may not be reliable because of shadowing from fluid in the retina^{73, 74} or because of pathologies
10 which disrupt normal retinal structures, such as macular hole, subretinal fluid, pigment
11 epithelium detachment and others.^{75, 76}

12
13 In cases where fully automated segmentation fails, C-mode visualization of structures may
14 augment subjective analyses.⁷⁷ A 3D volume of data can be sectioned in any plane after
15 acquisition, and for C-mode visualization, data are sectioned perpendicular to the retina. The
16 section can be of any thickness, so structures embedded within a volume can be exposed. Often,
17 since the true structure of the retina is curved, exact perpendicular sections slice through several
18 layers simultaneously,^{78, 79} so aligning the volume to structures such as the ILM or RPE assists
19 with isolating structures of interest.⁷⁷ Figure 4 shows an example C-mode section taken after
20 aligning a macular SD-OCT 3D volume to the RPE. By moving axially, past the retina and RPE,
21 choroidal blood vessels can be visualized. This is not apparent in the corresponding SD-OCT
22 fundus image because of highly reflective layers superficial to the choroid. C-mode provides
23 alternative viewing perspective for many retinal pathologies, such as cystoid macular edema,

1 central serous retinopathy, vitreoretinal traction, and age-related macular degeneration,⁷⁷ and this
2 can improve the visualization of these pathologies.

3

4 It is also possible to image the choroid by focusing the illuminating OCT beam deeper and
5 moving the choroid closer to zero delay.⁸⁰ In addition, longer wavelength imaging at $\sim 1\mu\text{m}$ ⁸¹
6 allows for deeper penetration of light into the retina and choroid. A combination of these
7 approaches may improve the current understanding of choroidal diseases.

8

9 Correcting ocular aberrations with adaptive-optics (AO)-OCT⁸² may also provide a unique
10 viewing perspective for retinal pathologies. This technique has been applied to view
11 photoreceptors⁸³ and RNFL.⁸⁴ The utility of longer wavelength imaging and AO-OCT is under
12 investigation and described in the Pre-clinical and Laboratory Studies section below.

13

14 **Anterior Segment**

15 Anterior segment OCT (AS-OCT) provides structural information of the cornea and anterior
16 chamber without contacting the eye, offering an ease of image acquisition and a considerable
17 advantage over ultrasound biomicroscopy (UBM). While it cannot be used to image deep
18 structures, such as the ciliary body, as UBM can, AS-OCT has higher axial resolution (5-10 μm
19 for AS-OCT as compared to 25 μm for UBM).⁸⁵

20

21 It is possible to acquire high-resolution images of the sclera, angle and iris with AS-OCT
22 imaging at longer wavelengths (1.3 μm).⁸⁶ High-resolution images of anterior chamber angle can

1 also be obtained using 850 nm systems, and this has lead to the visualization of the trabecular
2 meshwork and Schlemm's canal.⁸⁷⁻⁸⁹

3

4 Raster scanning and radial scanning of the cornea have been used to measure thickness,⁹⁰
5 resulting in reliable pachymetric mapping.^{91, 92} Pachymetric measurements obtained with AS-
6 OCT may assist with planning or follow-up of LASIK patients,⁹³ or used to diagnose
7 keratoconus.⁹⁴

8

9 In addition to its potential benefits in the evaluation of the anterior chamber angle and cornea,
10 AS-OCT has also been shown to be applicable in the assessment of lens thickness in phakic
11 eyes⁹⁵ or intracorneal ring placement.⁹⁶ This can provide an alternate, non-contact, method of
12 pre- and post-surgical assessment.

1 **Pre-clinical and Laboratory Studies**

2

3 **Swept-Source Optical Coherence Tomography and Longer Wavelength Imaging**

4 As previously discussed, SS-OCT obtains time-encoded spectral information by sweeping a
5 narrow bandwidth laser through a broad optical spectrum. Backscattered intensity is detected
6 with a photodetector. This is in contrast to SD-OCT, which uses a broad bandwidth light source
7 and detects the interference spectra with a CCD camera and spectrometer. While the use of
8 spectrometer-based SD-OCT has become widespread in the clinic, there are some benefits to
9 photodetector-based SS-OCT systems. Like SD-OCT, SS-OCT offers speed and sensitivity
10 advantages over TD-OCT.^{23,27} To date, speeds of up to 249,000A-scans/sec have been attained
11 in the eye.²⁷ This means that eye motion artifacts can be greatly reduced compared to TD-OCT.²²

12

13 One advantage of SS-OCT over SD-OCT is that it does not require a CCD camera and
14 spectrometer and instead uses a simpler photodetector.²⁷ A drawback to camera-based SD-OCT
15 detection is a drop-off in signal with depth of scanning due to the finite pixel size of the CCD
16 camera.^{25,97} While this can be improved by reducing the camera pixel size,⁹⁷ it increases the
17 complexity and therefore cost of the CCD array. A noticeable drop-off in signal with depth
18 typically does not occur with SS-OCT imaging due to the narrow bandwidth of the light
19 source.^{23,97}

20

21 At this time, one disadvantage of SS-OCT is that the majority of systems are now operating at
22 longer wavelengths ($\lambda=1-1.3 \mu\text{m}$), with very few studies demonstrating SS-OCT in the 800 nm
23 range.^{98,99} Water absorption limits the usable bandwidth at 1 μm and 1.3 μm ⁹⁹ and this limits the

1 axial resolution; the water absorption window at 850 nm is larger so higher axial resolution can
2 be achieved.

3

4 While axial resolution at longer wavelengths may not be as fine as at 850 nm, there are
5 advantages to using $\sim 1\mu\text{m}$ and $1.3\mu\text{m}$ sources. Posterior segment imaging using $\sim 1\mu\text{m}$ (1040-
6 1060nm)^{81, 100, 101} center wavelengths has allowed deeper penetration into the retina, optic nerve
7 head and choroid,^{81, 102} which may be beneficial for imaging choroidal vessels, lamina cribrosa
8 and pathologies such as choroidal neovascularization.¹⁰³ The water absorption window at $1.3\mu\text{m}$
9 offers even deeper penetration of light and may be useful for cornea and anterior segment
10 imaging.^{16, 22, 23, 104-106} Anterior chamber imaging at 1310 nm has been applied to visualize
11 anterior segment structures anterior and posterior to the iris, Schlemm's canal, trabecular
12 meshwork, and the scleral spur,¹⁰⁷ as well as the anterior chamber angle.¹⁰⁸

13

14 While SS-OCT systems at any wavelength are not yet commercially available for clinicians, in
15 part due to the cost of the light source, there is clinical potential for such devices. No signal drop-
16 off with depth in SS-OCT, in combination with deeper penetration from longer wavelengths,
17 may improve delineation of the outer retina, RPE and choroid thereby enhancing the
18 performance of segmentation algorithms. In addition, high speed $1.3\mu\text{m}$ imaging may be expand
19 the use of anterior segment OCT imaging.

20

21 **Adaptive Optics Optical Coherence Tomography**

22 Ophthalmic systems that employ adaptive optics (AO) dynamically adjust their optical
23 characteristics to compensate for monochromatic aberrations that occur naturally in the eye. AO

1 was initially proposed¹⁰⁹ and later employed by astronomers to correct distortions of light
2 passing through the atmosphere.¹¹⁰ In 1997, AO was demonstrated in the eye by Liang *et al*, who
3 used a Hartmann-Shack wavefront sensor and a deformable mirror to correct contrast sensitivity
4 and improve quality of vision for human subjects, and to obtain higher resolution images with an
5 AO-fundus camera.¹¹¹ Shortly thereafter, individual cone mosaics were imaged.¹¹²
6
7 AO-OCT was first reported by Miller *et al* in 2003⁸² to improve transverse resolution.
8 Uncorrected, conventional OCT beams 1 mm in diameter have a transverse resolution limited to
9 ~15-20 μm .¹¹³ This makes it difficult to visualize individual cellular structures. One way to
10 improve transverse resolution is to increase the numerical aperture, which in practice means
11 increasing the diameter of the OCT beam entering the eye, since this would decrease the spot
12 size on the retina. However, the theoretical diffraction-limited resolution cannot be attained due
13 to ocular aberrations¹¹⁴ that occur when the pupil is dilated.^{115, 116} AO-OCT measures and
14 corrects these aberrations using wavefront sensing and deformable mirrors, thereby minimizing
15 spot size and improving transverse resolution. It should also be noted that aberrations can also be
16 dependent on the bandwidth of the light source used for OCT imaging,¹¹⁶ and these may be
17 improved using an achromatizing lens.¹¹⁷
18
19 Ultrahigh (axial) resolution AO-OCT was presented in 2004, improving transverse resolution to
20 5-10 μm in the retina.¹¹³ Zhang *et al* developed an AO SD-OCT system and saw an enhancement
21 of the photoreceptor inner segment/outer segment junction *in-vivo* with AO.¹¹⁸ C-mode
22 sectioning of 3D datasets have also facilitated the visualization of axon bundles in the RNFL⁸⁴

1 and cone photoreceptor mosaics from healthy subjects,^{83, 119} and subjects with structural
2 abnormalities¹²⁰ and optic neuropathies.¹²¹

3
4 One disadvantage of AO imaging is that the depth of focus is narrow, which means focusing
5 simultaneously at different depths is difficult. For example, photoreceptors, located deep in the
6 retina, and superficial retinal ganglion cells cannot be brought into focus at the same time. This
7 may be able to be addressed by scanning in depth and varying the focal plane,¹²² or by stitching
8 together volumes.¹²³ Another limitation to AO imaging is that the field of view is restricted to
9 approximately 1-3 degrees; the use of an eye tracking system to acquire a series of neighboring
10 scans and gradually build up an image covering a larger volume may provide one solution to this
11 limitation.¹²⁴

12
13 One potential advantage of improved lateral resolution with AO-OCT is improved understanding
14 of normal and pathologic retinal function *in-vivo*. AO may also help improve the overall quality
15 of images obtained from eyes that have with more aberrations. Enhanced lateral resolution and
16 improved image quality may then lead to better performance of automated segmentation
17 algorithms and assist with disease diagnosis and follow-up.

18

19 **Polarization-Sensitive Optical Coherence Tomography**

20 Polarization-sensitive (PS)-OCT detects polarization changes in circularly polarized light.¹²⁵ PS-
21 OCT was initially applied to characterize the birefringence of tooth enamel,¹²⁶ skin,¹²⁷ and
22 cartilage.¹²⁸ In 2001, PS-OCT was first used in the eye¹²⁹ to measure birefringence of the RNFL
23 in rhesus monkeys. RNFL birefringence was measured in humans by Cense *et al*,⁴⁷⁻⁴⁹ who found

1 that, unlike RNFL thickness, birefringence does not change as a function of increasing radius
2 from the ONH.⁴⁸ It does, however, vary by sector around the ONH, with higher birefringence in
3 thicker areas.⁴⁸ Because birefringence may change with disease, RNFL birefringence obtained
4 with OCT may eventually provide an additional indicator of glaucomatous change. The utility of
5 PS-OCT in glaucoma detection and monitoring is currently under investigation. In addition to
6 measuring RNFL birefringence, a longer wavelength ($\lambda=1.3\mu\text{m}$) PS-OCT system has been used
7 to observe the anterior chamber in subjects after glaucoma surgery.¹⁰⁸ A swept-source PS-OCT
8 system at $1\mu\text{m}$ center wavelength was used to image sclera and lamina cribrosa,¹³⁰ which may
9 provide insight into structural changes occurring in the ONH in glaucoma.

10

11 Polarization of the RPE may be important in the detection of macular disease.^{131, 132} Gotzinger et
12 al developed a segmentation algorithm based on what they refer to as “polarization scrambling
13 effect” of the RPE,¹³² which provides an alternative to conventional intensity-based
14 quantification. A combined AO PS-OCT system was later used to measure RPE polarization
15 scrambling.¹³³ Conventional PS-OCT was used to observe subjects with AMD,^{134, 135} where
16 abnormal birefringence was co-localized with exudative lesions.

17

18 PS-OCT has been used for anterior segment imaging to measure corneal birefringence^{136, 137}, and
19 these measurements were used to compensate for corneal birefringence in retinal imaging.¹³⁸ A
20 difference in polarization in healthy corneas versus those with keratoconus was demonstrated *in*
21 *vitro*, suggesting PS-OCT may eventually provide insight into corneal pathologies *in-vivo*.¹³⁹

22

1 The aforementioned studies indicate that PS-OCT offers an alternative approach for detecting
2 changes of optical properties in tissue. If it can be established that a change in birefringence
3 occurs prior to tissue thinning or thickening, this may allow earlier detection and the opportunity
4 for earlier intervention.

5

6 **Eye-Tracking OCT Systems**

7 Subject eye motion can alter the intended location of an OCT scan. While attempts to correct eye
8 motion using post-processing methods are under development, real-time eye-tracking systems
9 may provide an alternate method for avoiding eye motion artifacts.⁴⁶ Menke et al showed that an
10 SD-OCT system with built-in eye tracking can provide reproducible measurements,¹⁴⁰ but it is
11 yet to be shown whether this yields higher reproducibility or better sensitivity and specificity
12 than devices without eye tracking systems.

13

14 **OCT Systems for Surgical Guidance**

15 As described earlier in this review, OCT is already being used for surgical planning and follow-
16 up. In addition, there has also been progress in the development of intraoperative OCT systems.
17 Intraoperative OCT was first demonstrated in anterior segment surgery, where a 1310 nm system
18 was coupled to an operating microscope.¹⁴¹ The use of a handheld OCT retinal imaging device
19 has also been demonstrated for use in patients undergoing vitrectomy, after removing either the
20 ILM or epiretinal membrane, in order to better visualize the macular pathology.¹⁴² It is possible
21 that the development of an intraoperative approach may be further improved using a projection
22 of a virtual OCT image over the surgical site and within the line of sight of the surgeon,¹⁴³ but
23 the implementation of this technique for surgery still have to be investigated.

1

2 **Animal OCT Imaging**

3 The noninvasive nature of image acquisition together with the commercialization of systems
4 optimized for laboratory use has resulted in a recent increase in the number of animal studies
5 using OCT. Two- and three-dimensional scanning with OCT is appealing because the same
6 animals can be followed over time, *in-vivo*, making longitudinal studies of ocular structures
7 possible without the need to sacrifice animals at various time points and obtain histological
8 sections. Not only does this reduce the number of animals required for experiments, but is
9 superior to cross-sectional experiments which require different animals for different time points.

10 The following briefly summarizes recent studies using OCT in animals, from small to large
11 animal models.

12

13 The eyes of small animal models commonly used in developmental biology, such as xenopus
14 laevis larvae¹⁴⁴ and zebrafish embryos¹⁴⁵ have successfully been imaged with OCT. Rodent
15 imaging with OCT is becoming increasingly popular given their relatively low cost and short
16 lifespan – and therefore shorter time for disease progression. In addition, many transgenic
17 models are easy for researchers to access. OCT has been used to study ocular dimensions¹⁴⁶ and
18 characterize normal eye growth¹⁴⁷ as well as growth of eyes in mouse models of myopia.¹⁴⁸
19 Mouse models of retinal degeneration have been imaged using TD-OCT,^{149, 150} and healthy and
20 degenerative mice with SD-OCT.¹⁵¹⁻¹⁵⁸

21

22 Recently, methods for automatically obtaining measurements from mouse OCT images have
23 been presented.^{159, 160} Images taken in an anesthetized mouse, held in place using a stage with a

1 glass cover slip to neutralize the strong refractive power of the mouse cornea were shown to be
2 reproducible.¹⁵⁹ This indicates that 3D SD-OCT imaging of the mouse retina may be useful for
3 longitudinal studies of retinal structure in mice.

4
5 Rats also provide an interesting platform for studying structural changes in the retina and optic
6 nerve in response to injury or disease. Given their larger eyes, it is less complicated to focus on
7 the retina than in the mouse. Retina and optic nerve imaging has been demonstrated in rat models
8 of retinal degeneration,¹⁵¹ retinal vein occlusion,¹⁶¹ retinal ganglion cell degeneration post nerve-
9 crush injury^{162, 163} and elevated intraocular pressure,¹⁶⁴ suggesting there is also potential for rats
10 to be used for longitudinal studies with OCT.

11
12 The eyes of larger animal models, such as chickens with retinal degeneration,¹⁶⁵ have been
13 imaged. Researchers have also used OCT to examine birds of prey,¹⁶⁶ pigs,^{167, 168} cats¹⁶⁹ and
14 rabbits.¹⁷⁰⁻¹⁷⁸ These animals have eyes that are comparable in size to the human eye, which
15 means large modifications of the OCT system optics are not necessary.

16
17 Nonhuman primate models are especially appealing for studies with OCT, since their ocular size
18 and structure closely matches the human eye. Nonhuman primate imaging may provide novel
19 insight into the mechanical damage to the RNFL and ONH associated with increased IOP, as is
20 often seen in glaucoma. PS-OCT has been used to look at birefringence of the RNFL,^{129, 179, 180}
21 and RNFL thickness was measured in eyes with unilateral, laser-induced ocular hypertension.^{181,}
22 ¹⁸² Strouthidis et al examined 3D SD-OCT images of the optic nerve in nonhuman primate
23 eyes.¹⁸³ They visualized the termination of Bruch's membrane, border tissue, and the anterior

1 scleral canal opening and showed that these structures correlated to disc photos¹⁸⁴ and
2 histology.¹⁸⁵ This set the stage for a study of alterations in the ONH that are due to increased
3 intraocular pressure.¹⁸⁶
4
5 Ultimately, longitudinal OCT studies of small and large animals may help evaluate the efficacy
6 of pharmacological agents, stem cell therapies, surgical intervention, and retinal prosthetics
7 while reducing the required number of animals. OCT has the potential to provide a better
8 understanding of disease development and progression in transgenic and other models of disease,
9 which may eventually translate to improved clinical assessment and understanding of disease.

1 **Conclusion**

2 The use of OCT imaging in ophthalmology has increased steadily in recent years, in part due to
3 technological improvements such as scanning speed, sensitivity and resolution. The field
4 continues to grow and transform the way glaucoma and retinal diseases are monitored. With 3D
5 imaging, there are new ways to visualize pathology and corresponding challenges to overcome.
6 Current approaches, such as RNFL thickness maps and C-mode visualization, attempt to
7 summarize structural information. These methods are not necessarily optimized for efficient
8 cross-sectional and longitudinal analysis, but with technological improvements such as longer
9 wavelength imaging, SS-OCT, AO-OCT, and PS-OCT on the horizon, even more structural
10 detail will be available. Translating these techniques to the clinic has already begun and many
11 could eventually be made available to the clinician. A combined slit-lamp/OCT system that
12 allows the clinician to access structural information during a routine examination may eventually
13 be available, as may a portable operating-room system. The use of OCT in animal models has
14 the potential to further understanding of disease while offering a platform for testing novel
15 approaches to treatment, as well as for innovations of the OCT technique itself. The future of
16 OCT is promising, but with some constraints that, if history is any indication, will become the
17 basis for future advancement.

1 References

- 2 1. Fercher AF, Menedoht K, Werner W. Eye-length measurement by interferometry with
3 partially coherent light. *Opt Lett* 1988;13:186-188.
- 4 2. Huang D, Swanson EA, Lin CP, et al. Optical coherence tomography. *Science*
5 1991;254:1178-1181.
- 6 3. Fercher AF, Hitzenberger CK, Drexler W, Kamp G, Sattmann H. In vivo optical
7 coherence tomography. *Am J Ophthalmol* 1993;116:113-114.
- 8 4. Puliafito CA, Hee MR, Lin CP, et al. Imaging of macular diseases with optical coherence
9 tomography. *Ophthalmology* 1995;102:217-229.
- 10 5. Hee MR, Izatt JA, Swanson EA, et al. Optical coherence tomography of the human
11 retina. *Arch Ophthalmol* 1995;113:325-332.
- 12 6. Izatt JA, Hee MR, Swanson EA, et al. Micrometer-scale resolution imaging of the
13 anterior eye in vivo with optical coherence tomography. *Arch Ophthalmol* 1994;112:1584-1589.
- 14 7. Swanson EA, Izatt JA, Hee MR, et al. In vivo retinal imaging by optical coherence
15 tomography. *Opt Lett* 1993;18:1864-1866.
- 16 8. Schuman JS, Hee MR, Arya AV, et al. Optical coherence tomography: a new tool for
17 glaucoma diagnosis. *Curr Opin Ophthalmol* 1995;6:89-95.
- 18 9. Schuman JS, Hee MR, Puliafito CA, et al. Quantification of nerve fiber layer thickness in
19 normal and glaucomatous eyes using optical coherence tomography. *Arch Ophthalmol*
20 1995;113:586-596.
- 21 10. Schuman JS, Pedut-Kloizman T, Hertzmark E, et al. Reproducibility of nerve fiber layer
22 thickness measurements using optical coherence tomography. *Ophthalmology* 1996;103:1889-
23 1898.
- 24 11. Drexler W, Morgner U, Kartner FX, et al. In vivo ultrahigh-resolution optical coherence
25 tomography. *Opt Lett* 1999;24:1221-1223.
- 26 12. Lim H, Jiang Y, Wang Y, Huang YC, Chen Z, Wise FW. Ultrahigh-resolution optical
27 coherence tomography with a fiber laser source at 1 microm. *Opt Lett* 2005;30:1171-1173.
- 28 13. Unterhuber A, Povazay B, Bizheva K, et al. Advances in broad bandwidth light sources
29 for ultrahigh resolution optical coherence tomography. *Phys Med Biol* 2004;49:1235-1246.
- 30 14. Wojtkowski M, Leitgeb R, Kowalczyk A, Bajraszewski T, Fercher A. In vivo human
31 retinal imaging by Fourier-domain optical coherence tomography. *J Biomed Opt* 2002;7:457-
32 463.
- 33 15. Fercher A, Hitzenberger C, Kamp G, Elzaiat S. Measurement of intraocular distances by
34 backscattering spectral interferometry. *Opt Commun* 1995;117:43-48.
- 35 16. Choma MA, Hsu K, Izatt JA. Swept source optical coherence tomography using an all-
36 fiber 1300-nm ring laser source. *J Biomed Opt* 2005;10:44009.
- 37 17. de Boer JF, Cense B, Park BH, Pierce MC, Tearney GJ, Bouma BE. Improved signal-to-
38 noise ratio in spectral-domain compared with time-domain optical coherence tomography. *Opt*
39 *Lett* 2003;28:2067-2069.
- 40 18. Leitgeb R, Wojtkowski M, Kowalczyk A, Hitzenberger CK, Sticker M, Fercher AF.
41 Spectral measurement of absorption by spectroscopic frequency-domain optical coherence
42 tomography. *Opt Lett* 2000;25:820-822.
- 43 19. Nassif N, Cense B, Park BH, et al. In vivo human retinal imaging by ultrahigh-speed
44 spectral domain optical coherence tomography. *Opt Lett* 2004;29:480-482.

- 1 20. Wojtkowski M, Srinivasan V, Fujimoto JG, et al. Three-dimensional retinal imaging with
2 high-speed ultrahigh-resolution optical coherence tomography. *Ophthalmology* 2005;112:1734-
3 1746.
- 4 21. Zhang J, Rao B, Chen Z. Swept source based fourier domain functional optical coherence
5 tomography. *Conf Proc IEEE Eng Med Biol Soc* 2005;7:7230-7233.
- 6 22. Yun SH, Tearney G, de Boer J, Bouma B. Pulsed-source and swept-source spectral-
7 domain optical coherence tomography with reduced motion artifacts. *Opt Express* 2004;12:5614-
8 5624.
- 9 23. Choma M, Sarunic M, Yang C, Izatt J. Sensitivity advantage of swept source and Fourier
10 domain optical coherence tomography. *Opt Express* 2003;11:2183-2189.
- 11 24. Drexler W, Morgner U, Ghanta RK, Kartner FX, Schuman JS, Fujimoto JG. Ultrahigh-
12 resolution ophthalmic optical coherence tomography. *Nat Med* 2001;7:502-507.
- 13 25. Leitgeb R, Hitzenberger C, Fercher A. Performance of fourier domain vs. time domain
14 optical coherence tomography. *Opt Express* 2003;11:889-894.
- 15 26. Potsaid B, Gorczynska I, Srinivasan VJ, et al. Ultrahigh speed spectral / Fourier domain
16 OCT ophthalmic imaging at 70,000 to 312,500 axial scans per second. *Opt Express*
17 2008;16:15149-15169.
- 18 27. Srinivasan VJ, Adler DC, Chen Y, et al. Ultrahigh-speed optical coherence tomography
19 for three-dimensional and en face imaging of the retina and optic nerve head. *Invest Ophthalmol*
20 *Vis Sci* 2008;49:5103-5110.
- 21 28. Bowd C, Weinreb RN, Williams JM, Zangwill LM. The retinal nerve fiber layer
22 thickness in ocular hypertensive, normal, and glaucomatous eyes with optical coherence
23 tomography. *Arch Ophthalmol* 2000;118:22-26.
- 24 29. Bowd C, Zangwill LM, Berry CC, et al. Detecting early glaucoma by assessment of
25 retinal nerve fiber layer thickness and visual function. *Invest Ophthalmol Vis Sci* 2001;42:1993-
26 2003.
- 27 30. Hoh ST, Greenfield DS, Mistlberger A, Liebmann JM, Ishikawa H, Ritch R. Optical
28 coherence tomography and scanning laser polarimetry in normal, ocular hypertensive, and
29 glaucomatous eyes. *Am J Ophthalmol* 2000;129:129-135.
- 30 31. Mistlberger A, Liebmann JM, Greenfield DS, et al. Heidelberg retina tomography and
31 optical coherence tomography in normal, ocular-hypertensive, and glaucomatous eyes.
32 *Ophthalmology* 1999;106:2027-2032.
- 33 32. Pieroth L, Schuman JS, Hertzmark E, et al. Evaluation of focal defects of the nerve fiber
34 layer using optical coherence tomography. *Ophthalmology* 1999;106:570-579.
- 35 33. Zangwill LM, Williams J, Berry CC, Knauer S, Weinreb RN. A comparison of optical
36 coherence tomography and retinal nerve fiber layer photography for detection of nerve fiber
37 layer damage in glaucoma. *Ophthalmology* 2000;107:1309-1315.
- 38 34. Wollstein G, Ishikawa H, Wang J, Beaton SA, Schuman JS. Comparison of three optical
39 coherence tomography scanning areas for detection of glaucomatous damage. *Am J Ophthalmol*
40 2005;139:39-43.
- 41 35. Schuman JS. Spectral domain optical coherence tomography for glaucoma (an AOS
42 thesis). *Trans Am Ophthalmol Soc* 2008;106:426-458.
- 43 36. Kim JS, Ishikawa H, Sung KR, et al. Retinal nerve fibre layer thickness measurement
44 reproducibility improved with spectral domain optical coherence tomography. *Br J Ophthalmol*
45 2009;93:1057-1063.

- 1 37. Gabriele ML, Ishikawa H, Wollstein G, et al. Peripapillary nerve fiber layer thickness
2 profile determined with high speed, ultrahigh resolution optical coherence tomography high-
3 density scanning. *Invest Ophthalmol Vis Sci* 2007;48:3154-3160.
- 4 38. Ishikawa H, Stein DM, Wollstein G, Beaton S, Fujimoto JG, Schuman JS. Macular
5 segmentation with optical coherence tomography. *Invest Ophthalmol Vis Sci* 2005;46:2012-
6 2017.
- 7 39. Kim JS, Ishikawa H, Gabriele ML, et al. Retinal nerve fiber layer thickness measurement
8 comparability between time domain optical coherence tomography (OCT) and spectral domain
9 OCT. *Invest Ophthalmol Vis Sci* 2010;51:896-902.
- 10 40. Jorgensen TM, Thomadsen J, Christensen U, Soliman W, Sander B. Enhancing the
11 signal-to-noise ratio in ophthalmic optical coherence tomography by image registration--method
12 and clinical examples. *J Biomed Opt* 2007;12:041208.
- 13 41. Ramrath L, Moreno G, Mueller H, Bonin T, Huettmann G, Schweikard A. Towards
14 multi-directional OCT for speckle noise reduction. *Med Image Comput Comput Assist Interv Int*
15 *Conf Med Image Comput Comput Assist Interv* 2008;11:815-823.
- 16 42. Ricco S, Chen M, Ishikawa H, Wollstein G, Schuman JS. Correcting Motion Artifacts in
17 Retinal Spectral Domain Optical Coherence Tomography via Image Registration *Medical Image*
18 *Computing and Computer-Assisted Intervention Proceedings* 2009;5761:100-107.
- 19 43. Xu J, Ishikawa H, Wollstein G, Schuman JS. Retinal vessel segmentation on SLO image.
20 *Conf Proc IEEE Eng Med Biol Soc* 2008;2008:2258-2261.
- 21 44. Ferguson RD, Hammer DX, Paunescu LA, Beaton S, Schuman JS. Tracking optical
22 coherence tomography. *Opt Lett* 2004;29:2139-2141.
- 23 45. Hammer DX, Ferguson RD, Magill JC, et al. Active retinal tracker for clinical optical
24 coherence tomography systems. *J Biomed Opt* 2005;10:024038.
- 25 46. Ishikawa H, Gabriele ML, Wollstein G, et al. Retinal nerve fiber layer assessment using
26 optical coherence tomography with active optic nerve head tracking. *Invest Ophthalmol Vis Sci*
27 2006;47:964-967.
- 28 47. Cense B, Chen TC, Park BH, Pierce MC, de Boer JF. In vivo birefringence and thickness
29 measurements of the human retinal nerve fiber layer using polarization-sensitive optical
30 coherence tomography. *J Biomed Opt* 2004;9:121-125.
- 31 48. Cense B, Chen TC, Park BH, Pierce MC, de Boer JF. Thickness and birefringence of
32 healthy retinal nerve fiber layer tissue measured with polarization-sensitive optical coherence
33 tomography. *Invest Ophthalmol Vis Sci* 2004;45:2606-2612.
- 34 49. Yamanari M, Miura M, Makita S, Yatagai T, Yasuno Y. Phase retardation measurement
35 of retinal nerve fiber layer by polarization-sensitive spectral-domain optical coherence
36 tomography and scanning laser polarimetry. *J Biomed Opt* 2008;13:014013.
- 37 50. Gupta V, Gupta P, Singh R, Dogra MR, Gupta A. Spectral-domain Cirrus high-definition
38 optical coherence tomography is better than time-domain Stratus optical coherence tomography
39 for evaluation of macular pathologic features in uveitis. *Am J Ophthalmol* 2008;145:1018-1022.
- 40 51. Koizumi H, Spaide RF, Fisher YL, Freund KB, Klancnik JM, Jr., Yannuzzi LA. Three-
41 dimensional evaluation of vitreomacular traction and epiretinal membrane using spectral-domain
42 optical coherence tomography. *Am J Ophthalmol* 2008;145:509-517.
- 43 52. Mojana F, Cheng L, Bartsch DU, et al. The role of abnormal vitreomacular adhesion in
44 age-related macular degeneration: spectral optical coherence tomography and surgical results.
45 *Am J Ophthalmol* 2008;146:218-227.

- 1 53. Punjabi OS, Flynn HW, Jr., Knighton RW, et al. Spectral domain optical coherence
2 tomography for proliferative diabetic retinopathy with subhyaloid hemorrhage. *Ophthalmic Surg*
3 *Lasers Imaging* 2008;39:494-496.
- 4 54. Schmidt-Erfurth U, Leitgeb RA, Michels S, et al. Three-dimensional ultrahigh-resolution
5 optical coherence tomography of macular diseases. *Invest Ophthalmol Vis Sci* 2005;46:3393-
6 3402.
- 7 55. Srinivasan VJ, Wojtkowski M, Witkin AJ, et al. High-definition and 3-dimensional
8 imaging of macular pathologies with high-speed ultrahigh-resolution optical coherence
9 tomography. *Ophthalmology* 2006;113:2054 e2051-2014.
- 10 56. Oh J, Smiddy WE, Flynn HW, Jr., Gregori G, Lujan B. Photoreceptor inner/outer
11 segment defect imaging by spectral domain OCT and visual prognosis after macular hole
12 surgery. *Invest Ophthalmol Vis Sci* 2010;51:1651-1658.
- 13 57. Sano M, Shimoda Y, Hashimoto H, Kishi S. Restored photoreceptor outer segment and
14 visual recovery after macular hole closure. *Am J Ophthalmol* 2009;147:313-318 e311.
- 15 58. Inoue M, Watanabe Y, Arakawa A, Sato S, Kobayashi S, Kadonosono K. Spectral-
16 domain optical coherence tomography images of inner/outer segment junctions and macular hole
17 surgery outcomes. *Graefes Arch Clin Exp Ophthalmol* 2009;247:325-330.
- 18 59. Chung EJ, Lew YJ, Lee H, Koh HJ. OCT-guided hyaloid release for vitreomacular
19 traction syndrome. *Korean J Ophthalmol* 2008;22:169-173.
- 20 60. Falkner-Radler CI, Glittenberg C, Binder S. Spectral domain high-definition optical
21 coherence tomography in patients undergoing epiretinal membrane surgery. *Ophthalmic Surg*
22 *Lasers Imaging* 2009;40:270-276.
- 23 61. Michalewska Z, Michalewski J, Cisiecki S, Adelman R, Nawrocki J. Correlation between
24 foveal structure and visual outcome following macular hole surgery: a spectral optical coherence
25 tomography study. *Graefes Arch Clin Exp Ophthalmol* 2008;246:823-830.
- 26 62. Uchino E, Uemura A, Doi N, Ohba N. Postsurgical evaluation of idiopathic
27 vitreomacular traction syndrome by optical coherence tomography. *Am J Ophthalmol*
28 2001;132:122-123.
- 29 63. Chang LK, Fine HF, Spaide RF, Koizumi H, Grossniklaus HE. Ultrastructural correlation
30 of spectral-domain optical coherence tomographic findings in vitreomacular traction syndrome.
31 *Am J Ophthalmol* 2008;146:121-127.
- 32 64. Sayegh RG, Georgopoulos M, Geitzenauer W, Simader C, Kiss C, Schmidt-Erfurth U.
33 High-Resolution Optical Coherence Tomography after Surgery for Vitreomacular Traction A 2-
34 Year Follow-up. *Ophthalmology* 2010.
- 35 65. Freeman SR, Kozak I, Cheng L, et al. Optical coherence tomography-raster scanning and
36 manual segmentation in determining drusen volume in age-related macular degeneration. *Retina*
37 2010;30:431-435.
- 38 66. Yi K, Mujat M, Park BH, et al. Spectral domain optical coherence tomography for
39 quantitative evaluation of drusen and associated structural changes in non-neovascular age-
40 related macular degeneration. *Br J Ophthalmol* 2009;93:176-181.
- 41 67. Cabrera DeBuc D, Somfai GM. Early detection of retinal thickness changes in diabetes
42 using Optical Coherence Tomography. *Med Sci Monit* 16:MT15-21.
- 43 68. van Dijk HW, Kok PH, Garvin M, et al. Selective loss of inner retinal layer thickness in
44 type 1 diabetic patients with minimal diabetic retinopathy. *Invest Ophthalmol Vis Sci*
45 2009;50:3404-3409.

- 1 69. Huang J, Liu X, Wu Z, et al. Macular and Retinal Nerve Fiber Layer Thickness
2 Measurements in Normal Eyes With the Stratus OCT, the Cirrus HD-OCT, and the Topcon 3D
3 OCT-1000. *J Glaucoma* 2010.
- 4 70. Koleva-Georgieva D, Sivkova N. Assessment of serous macular detachment in eyes with
5 diabetic macular edema by use of spectral-domain optical coherence tomography. *Graefes Arch*
6 *Clin Exp Ophthalmol* 2009;247:1461-1469.
- 7 71. Arichika S, Hangai M, Yoshimura N. Correlation between thickening of the inner and
8 outer retina and visual acuity in patients with epiretinal membrane. *Retina* 2010;30:503-508.
- 9 72. Nunes S, Pereira I, Santos A, Bernardes R, Cunha-Vaz J. Central retinal thickness
10 measured with HD-OCT shows a weak correlation with visual acuity in eyes with CSME. *Br J*
11 *Ophthalmol* 2010;94:1201-1204.
- 12 73. Patel PJ, Chen FK, da Cruz L, Tufail A. Segmentation error in Stratus optical coherence
13 tomography for neovascular age-related macular degeneration. *Invest Ophthalmol Vis Sci*
14 2009;50:399-404.
- 15 74. Sadda SR, Wu Z, Walsh AC, et al. Errors in retinal thickness measurements obtained by
16 optical coherence tomography. *Ophthalmology* 2006;113:285-293.
- 17 75. Keane PA, Mand PS, Liakopoulos S, Walsh AC, Sadda SR. Accuracy of retinal thickness
18 measurements obtained with Cirrus optical coherence tomography. *Br J Ophthalmol*
19 2009;93:1461-1467.
- 20 76. Giani A, Cigada M, Esmaili DD, et al. Artifacts in automatic retinal segmentation using
21 different optical coherence tomography instruments. *Retina* 2010;30:607-616.
- 22 77. Ishikawa H, Kim J, Friberg TR, et al. Three-dimensional optical coherence tomography
23 (3D-OCT) image enhancement with segmentation-free contour modeling C-mode. *Invest*
24 *Ophthalmol Vis Sci* 2009;50:1344-1349.
- 25 78. Alam S, Zawadzki RJ, Choi S, et al. Clinical application of rapid serial fourier-domain
26 optical coherence tomography for macular imaging. *Ophthalmology* 2006;113:1425-1431.
- 27 79. Cucu RG, Podoleanu AG, Rogers JA, Pedro J, Rosen RB. Combined confocal/en face T-
28 scan-based ultrahigh-resolution optical coherence tomography in vivo retinal imaging. *Opt Lett*
29 2006;31:1684-1686.
- 30 80. Spaide RF, Koizumi H, Pozzoni MC. Enhanced depth imaging spectral-domain optical
31 coherence tomography. *Am J Ophthalmol* 2008;146:496-500.
- 32 81. Lee EC, de Boer JF, Mujat M, Lim H, Yun SH. In vivo optical frequency domain
33 imaging of human retina and choroid. *Opt Express* 2006;14:4403-4411.
- 34 82. Miller DT, Qu J, Jonnal RS, Thorn K. Coherence gating and adaptive optics in the eye.
35 In: Tuchin VV, Izatt JA, Fujimoto JG (eds), *Coherence Domain Methods and Optical Coherence*
36 *Tomography in Biomedicine VII, Proc SPIE 4596*; 2003:65-72.
- 37 83. Zawadzki RJ, Jones SM, Olivier SS, et al. Adaptive-optics optical coherence tomography
38 for high-resolution and high-speed 3D retinal in vivo imaging. *Opt Express* 2005;13:8532-8546.
- 39 84. Zawadzki RJ, Choi SS, Jones SM, Oliver SS, Werner JS. Adaptive optics-optical
40 coherence tomography: optimizing visualization of microscopic retinal structures in three
41 dimensions. *J Opt Soc Am A Opt Image Sci Vis* 2007;24:1373-1383.
- 42 85. Nolan W. Anterior segment imaging: ultrasound biomicroscopy and anterior segment
43 optical coherence tomography. *Curr Opin Ophthalmol* 2008;19:115-121.
- 44 86. Radhakrishnan S, Rollins AM, Roth JE, et al. Real-time optical coherence tomography of
45 the anterior segment at 1310 nm. *Arch Ophthalmol* 2001;119:1179-1185.

- 1 87. Huang D, Li Y, Radhakrishnan S. Optical coherence tomography of the anterior segment
2 of the eye. *Ophthalmol Clin North Am* 2004;17:1-6.
- 3 88. Kagemann L, Wollstein G, Ishikawa H, et al. Identification and assessment of Schlemm's
4 canal by spectral-domain optical coherence tomography. *Invest Ophthalmol Vis Sci*
5 2010;51:4054-4059.
- 6 89. Radhakrishnan S, Huang D, Smith SD. Optical coherence tomography imaging of the
7 anterior chamber angle. *Ophthalmol Clin North Am* 2005;18:375-381, vi.
- 8 90. Tang M, Li Y, Avila M, Huang D. Measuring total corneal power before and after laser
9 in situ keratomileusis with high-speed optical coherence tomography. *J Cataract Refract Surg*
10 2006;32:1843-1850.
- 11 91. Li Y, Shekhar R, Huang D. Corneal pachymetry mapping with high-speed optical
12 coherence tomography. *Ophthalmology* 2006;113:792-799 e792.
- 13 92. Li Y, Tang M, Zhang X, Salaroli CH, Ramos JL, Huang D. Pachymetric mapping with
14 Fourier-domain optical coherence tomography. *J Cataract Refract Surg* 2010;36:826-831.
- 15 93. Li Y, Netto MV, Shekhar R, Krueger RR, Huang D. A longitudinal study of LASIK flap
16 and stromal thickness with high-speed optical coherence tomography. *Ophthalmology*
17 2007;114:1124-1132.
- 18 94. Li Y, Meisler DM, Tang M, et al. Keratoconus diagnosis with optical coherence
19 tomography pachymetry mapping. *Ophthalmology* 2008;115:2159-2166.
- 20 95. Zeng Y, Liu Y, Liu X, et al. Comparison of lens thickness measurements using the
21 anterior segment optical coherence tomography and A-scan ultrasonography. *Invest Ophthalmol*
22 *Vis Sci* 2009;50:290-294.
- 23 96. Christopoulos V, Kagemann L, Wollstein G, et al. In vivo corneal high-speed, ultra high-
24 resolution optical coherence tomography. *Arch Ophthalmol* 2007;125:1027-1035.
- 25 97. Yaqoob Z, Wu J, Yang C. Spectral domain optical coherence tomography: a better OCT
26 imaging strategy. *Biotechniques* 2005;39:S6-13.
- 27 98. Lim H, Mujat M, Kerbage C, et al. High-speed imaging of human retina in vivo with
28 swept-source optical coherence tomography. *Opt Express* 2006;14:12902-12908.
- 29 99. Srinivasan VJ, Huber R, Gorczynska I, et al. High-speed, high-resolution optical
30 coherence tomography retinal imaging with a frequency-swept laser at 850 nm. *Opt Lett*
31 2007;32:361-363.
- 32 100. de Bruin DM, Burnes DL, Loewenstein J, et al. In vivo three-dimensional imaging of
33 neovascular age-related macular degeneration using optical frequency domain imaging at 1050
34 nm. *Invest Ophthalmol Vis Sci* 2008;49:4545-4552.
- 35 101. Yasuno Y, Hong Y, Makita S, et al. In vivo high-contrast imaging of deep posterior eye
36 by 1-microm swept source optical coherence tomography and scattering optical coherence
37 angiography. *Opt Express* 2007;15:6121-6139.
- 38 102. Povazay B, Hermann B, Unterhuber A, et al. Three-dimensional optical coherence
39 tomography at 1050 nm versus 800 nm in retinal pathologies: enhanced performance and
40 choroidal penetration in cataract patients. *J Biomed Opt* 2007;12:041211.
- 41 103. Yasuno Y, Miura M, Kawana K, et al. Visualization of sub-retinal pigment epithelium
42 morphologies of exudative macular diseases by high-penetration optical coherence tomography.
43 *Invest Ophthalmol Vis Sci* 2009;50:405-413.
- 44 104. Yun S, Tearney G, de Boer J, Iftimia N, Bouma B. High-speed optical frequency-domain
45 imaging. *Opt Express* 2003;11:2953-2963.

- 1 105. Yasuno Y, Madjarova VD, Makita S, et al. Three-dimensional and high-speed swept-
2 source optical coherence tomography for in vivo investigation of human anterior eye segments.
3 *Opt Express* 2005;13:10652-10664.
- 4 106. Miura M, Mori H, Watanabe Y, et al. Three-dimensional optical coherence tomography
5 of granular corneal dystrophy. *Cornea* 2007;26:373-374.
- 6 107. Asrani S, Sarunic M, Santiago C, Izatt J. Detailed visualization of the anterior segment
7 using fourier-domain optical coherence tomography. *Arch Ophthalmol* 2008;126:765-771.
- 8 108. Yasuno Y, Yamanari M, Kawana K, Oshika T, Miura M. Investigation of post-glaucoma-
9 surgery structures by three-dimensional and polarization sensitive anterior eye segment optical
10 coherence tomography. *Opt Express* 2009;17:3980-3996.
- 11 109. Babcock HW. The possibility of compensating astronomical seeing. *Publ Astron Soc Pac*
12 1953;65:229-236.
- 13 110. Hardy JW. Adaptive optics: a new technology for the control of light. *Proc IEEE*
14 1978;66:651-697.
- 15 111. Liang J, Williams DR, Miller DT. Supernormal vision and high-resolution retinal
16 imaging through adaptive optics. *J Opt Soc Am A Opt Image Sci Vis* 1997;14:2884-2892.
- 17 112. Roorda A, Williams DR. The arrangement of the three cone classes in the living human
18 eye. *Nature* 1999;397:520-522.
- 19 113. Hermann B, Fernandez EJ, Unterhuber A, et al. Adaptive-optics ultrahigh-resolution
20 optical coherence tomography. *Opt Lett* 2004;29:2142-2144.
- 21 114. Donnelly WJ, 3rd, Roorda A. Optimal pupil size in the human eye for axial resolution. *J*
22 *Opt Soc Am A Opt Image Sci Vis* 2003;20:2010-2015.
- 23 115. Artal P, Guirao A, Berrio E, Williams DR. Compensation of corneal aberrations by the
24 internal optics in the human eye. *J Vis* 2001;1:1-8.
- 25 116. Fernandez E, Drexler W. Influence of ocular chromatic aberration and pupil size on
26 transverse resolution in ophthalmic adaptive optics optical coherence tomography. *Opt Express*
27 2005;13:8184-8197.
- 28 117. Fernandez EJ, Unterhuber A, Povazay B, Hermann B, Artal P, Drexler W. Chromatic
29 aberration correction of the human eye for retinal imaging in the near infrared. *Opt Express*
30 2006;14:6213-6225.
- 31 118. Zhang Y, Rha J, Jonnal R, Miller D. Adaptive optics parallel spectral domain optical
32 coherence tomography for imaging the living retina. *Opt Express* 2005;13:4792-4811.
- 33 119. Zhang Y, Cense B, Rha J, et al. High-speed volumetric imaging of cone photoreceptors
34 with adaptive optics spectral-domain optical coherence tomography. *Opt Express* 2006;14:4380-
35 4394.
- 36 120. Hammer DX, Iftimia NV, Ferguson RD, et al. Foveal fine structure in retinopathy of
37 prematurity: an adaptive optics Fourier domain optical coherence tomography study. *Invest*
38 *Ophthalmol Vis Sci* 2008;49:2061-2070.
- 39 121. Choi SS, Zawadzki RJ, Keltner JL, Werner JS. Changes in cellular structures revealed by
40 ultra-high resolution retinal imaging in optic neuropathies. *Invest Ophthalmol Vis Sci*
41 2008;49:2103-2119.
- 42 122. Fernandez EJ, Povazay B, Hermann B, et al. Three-dimensional adaptive optics
43 ultrahigh-resolution optical coherence tomography using a liquid crystal spatial light modulator.
44 *Vision Res* 2005;45:3432-3444.

- 1 123. Zawadzki RJ, Choi SS, Fuller AR, Evans JW, Hamann B, Werner JS. Cellular resolution
2 volumetric in vivo retinal imaging with adaptive optics-optical coherence tomography. *Opt*
3 *Express* 2009;17:4084-4094.
- 4 124. Burns SA, Tumber R, Elsner AE, Ferguson D, Hammer DX. Large-field-of-view,
5 modular, stabilized, adaptive-optics-based scanning laser ophthalmoscope. *J Opt Soc Am A Opt*
6 *Image Sci Vis* 2007;24:1313-1326.
- 7 125. de Boer JF, Milner TE, van Gemert MJ, Nelson JS. Two-dimensional birefringence
8 imaging in biological tissue by polarization-sensitive optical coherence tomography. *Opt Lett*
9 1997;22:934-936.
- 10 126. Wang XJ, Milner TE, de Boer JF, Zhang Y, Pashley DH, Nelson JS. Characterization of
11 dentin and enamel by use of optical coherence tomography. *Appl Opt* 1999;38:2092-2096.
- 12 127. Saxer CE, de Boer JF, Park BH, Zhao Y, Chen Z, Nelson JS. High-speed fiber based
13 polarization-sensitive optical coherence tomography of in vivo human skin. *Opt Lett*
14 2000;25:1355-1357.
- 15 128. Drexler W, Stamper D, Jesser C, et al. Correlation of collagen organization with
16 polarization sensitive imaging of in vitro cartilage: implications for osteoarthritis. *J Rheumatol*
17 2001;28:1311-1318.
- 18 129. Ducros MG, Marsack JD, Rylander HG, 3rd, Thomsen SL, Milner TE. Primate retina
19 imaging with polarization-sensitive optical coherence tomography. *J Opt Soc Am A Opt Image*
20 *Sci Vis* 2001;18:2945-2956.
- 21 130. Yamanari M, Lim Y, Makita S, Yasuno Y. Visualization of phase retardation of deep
22 posterior eye by polarization-sensitive swept-source optical coherence tomography with 1-
23 microm probe. *Opt Express* 2009;17:12385-12396.
- 24 131. Pircher M, Gotzinger E, Findl O, et al. Human macula investigated in vivo with
25 polarization-sensitive optical coherence tomography. *Invest Ophthalmol Vis Sci* 2006;47:5487-
26 5494.
- 27 132. Gotzinger E, Pircher M, Geitzenauer W, et al. Retinal pigment epithelium segmentation
28 by polarization sensitive optical coherence tomography. *Opt Express* 2008;16:16410-16422.
- 29 133. Cense B, Gao W, Brown JM, et al. Retinal imaging with polarization-sensitive optical
30 coherence tomography and adaptive optics. *Opt Express* 2009;17:21634-21651.
- 31 134. Miura M, Yamanari M, Iwasaki T, et al. Imaging polarimetry in age-related macular
32 degeneration. *Invest Ophthalmol Vis Sci* 2008;49:2661-2667.
- 33 135. Ahlers C, Gotzinger E, Pircher M, et al. Imaging of the retinal pigment epithelium in age-
34 related macular degeneration using polarization-sensitive optical coherence tomography. *Invest*
35 *Ophthalmol Vis Sci* 2010;51:2149-2157.
- 36 136. Gotzinger E, Pircher M, Sticker M, Fercher AF, Hitzenberger CK. Measurement and
37 imaging of birefringent properties of the human cornea with phase-resolved, polarization-
38 sensitive optical coherence tomography. *J Biomed Opt* 2004;9:94-102.
- 39 137. Hitzenberger CK, Gotzinger E, Pircher M. Birefringence properties of the human cornea
40 measured with polarization sensitive optical coherence tomography. *Bull Soc Belge Ophthalmol*
41 2006;153-168.
- 42 138. Pircher M, Gotzinger E, Baumann B, Hitzenberger CK. Corneal birefringence
43 compensation for polarization sensitive optical coherence tomography of the human retina. *J*
44 *Biomed Opt* 2007;12:041210.

- 1 139. Gotzinger E, Pircher M, Dejaco-Ruhswurm I, Kaminski S, Skorpik C, Hitzenberger CK.
2 Imaging of birefringent properties of keratoconus corneas by polarization-sensitive optical
3 coherence tomography. *Invest Ophthalmol Vis Sci* 2007;48:3551-3558.
- 4 140. Menke MN, Dabov S, Knecht P, Sturm V. Reproducibility of retinal thickness
5 measurements in healthy subjects using spectralis optical coherence tomography. *Am J*
6 *Ophthalmol* 2009;147:467-472.
- 7 141. Geerling G, Muller M, Winter C, et al. Intraoperative 2-dimensional optical coherence
8 tomography as a new tool for anterior segment surgery. *Arch Ophthalmol* 2005;123:253-257.
- 9 142. Dayani PN, Maldonado R, Farsiu S, Toth CA. Intraoperative use of handheld spectral
10 domain optical coherence tomography imaging in macular surgery. *Retina* 2009;29:1457-1468.
- 11 143. Galeotti J, Sajjad A, Wang B, et al. The OCT penlight: In-situ image guidance for
12 microsurgery. *SPIE Medical Imaging 2010* 2010.
- 13 144. Boppart SA, Brezinski ME, Bouma BE, Tearney GJ, Fujimoto JG. Investigation of
14 developing embryonic morphology using optical coherence tomography. *Dev Biol* 1996;177:54-
15 63.
- 16 145. Kagemann L, Ishikawa H, Zou J, et al. Repeated, noninvasive, high resolution spectral
17 domain optical coherence tomography imaging of zebrafish embryos. *Mol Vis* 2008;14:2157-
18 2170.
- 19 146. Zhou X, Xie J, Shen M, et al. Biometric measurement of the mouse eye using optical
20 coherence tomography with focal plane advancement. *Vision Res* 2008;48:1137-1143.
- 21 147. Zhou X, Shen M, Xie J, et al. The development of the refractive status and ocular growth
22 in C57BL/6 mice. *Invest Ophthalmol Vis Sci* 2008;49:5208-5214.
- 23 148. Zhou X, Huang Q, An J, et al. Genetic Deletion of the Adenosine A2A Receptor Confers
24 Postnatal Development of Relative Myopia in Mice. *Invest Ophthalmol Vis Sci* 2010.
- 25 149. Horio N, Kachi S, Hori K, et al. Progressive change of optical coherence tomography
26 scans in retinal degeneration slow mice. *Arch Ophthalmol* 2001;119:1329-1332.
- 27 150. Li Q, Timmers AM, Hunter K, et al. Noninvasive imaging by optical coherence
28 tomography to monitor retinal degeneration in the mouse. *Invest Ophthalmol Vis Sci*
29 2001;42:2981-2989.
- 30 151. Srinivasan VJ, Ko TH, Wojtkowski M, et al. Noninvasive volumetric imaging and
31 morphometry of the rodent retina with high-speed, ultrahigh-resolution optical coherence
32 tomography. *Invest Ophthalmol Vis Sci* 2006;47:5522-5528.
- 33 152. Kocaoglu OP, Uhlhorn SR, Hernandez E, et al. Simultaneous fundus imaging and optical
34 coherence tomography of the mouse retina. *Invest Ophthalmol Vis Sci* 2007;48:1283-1289.
- 35 153. Kim KH, Puoris'haag M, Maguluri GN, et al. Monitoring mouse retinal degeneration
36 with high-resolution spectral-domain optical coherence tomography. *J Vis* 2008;8:17 11-11.
- 37 154. Fingler J, Readhead C, Schwartz DM, Fraser SE. Phase-contrast OCT imaging of
38 transverse flows in the mouse retina and choroid. *Invest Ophthalmol Vis Sci* 2008;49:5055-5059.
- 39 155. Huber G, Beck SC, Grimm C, et al. Spectral domain optical coherence tomography in
40 mouse models of retinal degeneration. *Invest Ophthalmol Vis Sci* 2009;50:5888-5895.
- 41 156. Xu J, Molday LL, Molday RS, Sarunic MV. In vivo imaging of the mouse model of X-
42 linked juvenile retinoschisis with fourier domain optical coherence tomography. *Invest*
43 *Ophthalmol Vis Sci* 2009;50:2989-2993.
- 44 157. Maeda A, Golczak M, Maeda T, Palczewski K. Limited roles of Rdh8, Rdh12, and
45 Abca4 in all-trans-retinal clearance in mouse retina. *Invest Ophthalmol Vis Sci* 2009;50:5435-
46 5443.

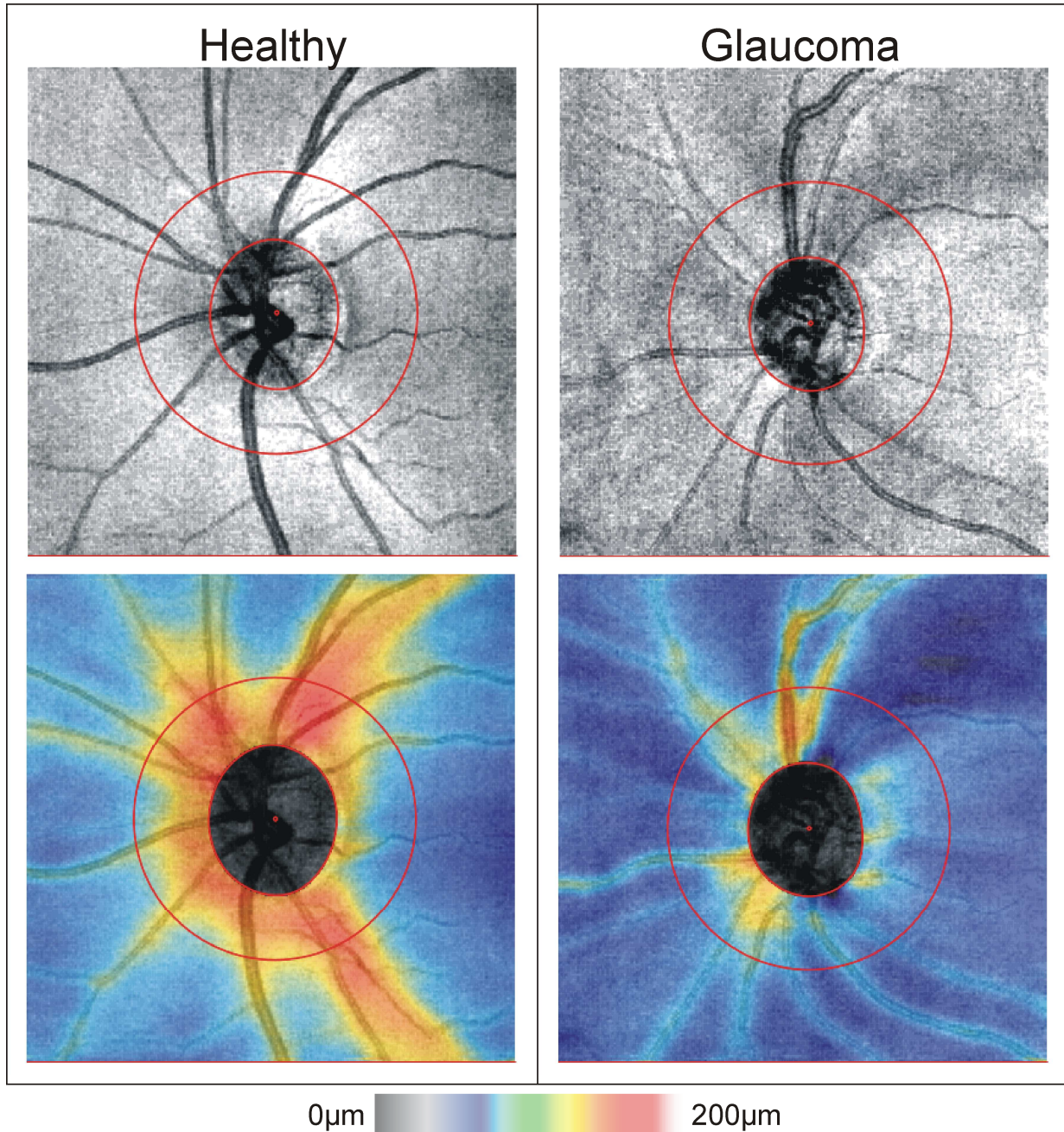
- 1 158. Fischer MD, Huber G, Beck SC, et al. Noninvasive, in vivo assessment of mouse retinal
2 structure using optical coherence tomography. *PLoS One* 2009;4:e7507.
- 3 159. Gabriele ML, Ishikawa H, Schuman JS, et al. Reproducibility of Spectral-Domain
4 Optical Coherence Tomography Total Retinal Thickness Measurements in Mice. *Invest*
5 *Ophthalmol Vis Sci* 2010.
- 6 160. Ruggeri M, Tsechpenakis G, Jiao S, et al. Retinal tumor imaging and volume
7 quantification in mouse model using spectral-domain optical coherence tomography. *Opt*
8 *Express* 2009;17:4074-4083.
- 9 161. Doukas J, Mahesh S, Umeda N, et al. Topical administration of a multi-targeted kinase
10 inhibitor suppresses choroidal neovascularization and retinal edema. *J Cell Physiol* 2008;216:29-
11 37.
- 12 162. Bai Y, Xu J, Brahim F, Zhuo Y, Sarunic MV, Saragovi HU. An agonistic anti-TrkB
13 mAb, but not BDNF, causes sustained TrkB activation, delays RGC death, and protects the
14 retinal structure in optic nerve axotomy and in glaucoma. *Invest Ophthalmol Vis Sci* 2010.
- 15 163. Nagata A, Higashide T, Ohkubo S, Takeda H, Sugiyama K. In vivo quantitative
16 evaluation of the rat retinal nerve fiber layer with optical coherence tomography. *Invest*
17 *Ophthalmol Vis Sci* 2009;50:2809-2815.
- 18 164. Guo L, Tsaturian V, Luong V, et al. En face optical coherence tomography: a new
19 method to analyse structural changes of the optic nerve head in rat glaucoma. *Br J Ophthalmol*
20 2005;89:1210-1216.
- 21 165. Huang Y, Cideciyan AV, Papastergiou GI, et al. Relation of optical coherence
22 tomography to microanatomy in normal and rd chickens. *Invest Ophthalmol Vis Sci*
23 1998;39:2405-2416.
- 24 166. Ruggeri M, Major JC, McKeown C, Knighton RW, Puliafito CA, Jiao S. Retinal
25 Structure of Birds of Prey Revealed by Ultra-High Resolution Spectral-Domain Optical
26 Coherence Tomography. *Invest Ophthalmol Vis Sci* 2010.
- 27 167. Gloesmann M, Hermann B, Schubert C, Sattmann H, Ahnelt PK, Drexler W. Histologic
28 correlation of pig retina radial stratification with ultrahigh-resolution optical coherence
29 tomography. *Invest Ophthalmol Vis Sci* 2003;44:1696-1703.
- 30 168. Gekeler F, Szurman P, Grisanti S, et al. Compound subretinal prostheses with extra-
31 ocular parts designed for human trials: successful long-term implantation in pigs. *Graefes Arch*
32 *Clin Exp Ophthalmol* 2007;45:230-241.
- 33 169. Gekeler F, Gmeiner H, Volker M, et al. Assessment of the posterior segment of the cat
34 eye by optical coherence tomography (OCT). *Vet Ophthalmol* 2007;10:173-178.
- 35 170. Kim ET, Kim C, Lee SW, Seo JM, Chung H, Kim SJ. Feasibility of microelectrode array
36 (MEA) based on silicone-polyimide hybrid for retina prosthesis. *Invest Ophthalmol Vis Sci*
37 2009;50:4337-4341.
- 38 171. Cong L, Sun D, Zhang Z, Jiao W, Rizzolo LJ, Peng S. A novel rabbit model for studying
39 RPE transplantation. *Invest Ophthalmol Vis Sci* 2008;49:4115-4125.
- 40 172. Ameri H, Kim JG, Ratanapakorn T, Chader GJ, Humayun MS. Intravitreal and subretinal
41 injection of tissue plasminogen activator (tPA) in the treatment of experimentally created retinal
42 vein occlusion in rabbits. *Retina* 2008;28:350-355.
- 43 173. Ameri H, Chader GJ, Kim JG, Sadda SR, Rao NA, Humayun MS. The effects of
44 intravitreal bevacizumab on retinal neovascular membrane and normal capillaries in rabbits.
45 *Invest Ophthalmol Vis Sci* 2007;48:5708-5715.

- 1 174. Qiu G, Stewart JM, Sadda S, et al. A new model of experimental subretinal
2 neovascularization in the rabbit. *Exp Eye Res* 2006;83:141-152.
- 3 175. Kozak I, Cheng L, Mendez T, Davidson MC, Freeman WR. Evaluation of the toxicity of
4 subretinal triamcinolone acetonide in the rabbit. *Retina* 2006;26:811-817.
- 5 176. Asejczyk-Widlicka M, Schachar RA, Pierscionek BK. Optical coherence tomography
6 measurements of the fresh porcine eye and response of the outer coats of the eye to volume
7 increase. *J Biomed Opt* 2008;13:024002.
- 8 177. Reiser BJ, Ignacio TS, Wang Y, et al. In vitro measurement of rabbit corneal epithelial
9 thickness using ultrahigh resolution optical coherence tomography. *Vet Ophthalmol* 2005;8:85-
10 88.
- 11 178. Hosseini K, Kholodnykh AI, Petrova IY, Esenaliev RO, Hendrikse F, Motamedi M.
12 Monitoring of rabbit cornea response to dehydration stress by optical coherence tomography.
13 *Invest Ophthalmol Vis Sci* 2004;45:2555-2562.
- 14 179. Kemp NJ, Park J, Zaatari HN, Rylander HG, Milner TE. High-sensitivity determination
15 of birefringence in turbid media with enhanced polarization-sensitive optical coherence
16 tomography. *J Opt Soc Am A Opt Image Sci Vis* 2005;22:552-560.
- 17 180. Rylander HG, 3rd, Kemp NJ, Park J, Zaatari HN, Milner TE. Birefringence of the
18 primate retinal nerve fiber layer. *Exp Eye Res* 2005;81:81-89.
- 19 181. Harwerth RS, Vilupuru AS, Rangaswamy NV, Smith EL, 3rd. The relationship between
20 nerve fiber layer and perimetry measurements. *Invest Ophthalmol Vis Sci* 2007;48:763-773.
- 21 182. Schuman JS, Pedut-Kloizman T, Pakter H, et al. Optical coherence tomography and
22 histologic measurements of nerve fiber layer thickness in normal and glaucomatous monkey
23 eyes. *Invest Ophthalmol Vis Sci* 2007;48:3645-3654.
- 24 183. Strouthidis NG, Yang H, Fortune B, Downs JC, Burgoyne CF. Detection of optic nerve
25 head neural canal opening within histomorphometric and spectral domain optical coherence
26 tomography data sets. *Invest Ophthalmol Vis Sci* 2009;50:214-223.
- 27 184. Strouthidis NG, Yang H, Reynaud JF, et al. Comparison of clinical and spectral domain
28 optical coherence tomography optic disc margin anatomy. *Invest Ophthalmol Vis Sci*
29 2009;50:4709-4718.
- 30 185. Strouthidis NG, Grimm J, Williams GA, Cull GA, Wilson DJ, Burgoyne CF. A
31 comparison of optic nerve head morphology viewed by spectral domain optical coherence
32 tomography and by serial histology. *Invest Ophthalmol Vis Sci* 2010;51:1464-1474.
- 33 186. Fortune B, Yang H, Strouthidis NG, et al. The effect of acute intraocular pressure
34 elevation on peripapillary retinal thickness, retinal nerve fiber layer thickness, and retardance.
35 *Invest Ophthalmol Vis Sci* 2009;50:4719-4726.

1 **Figure Legends**

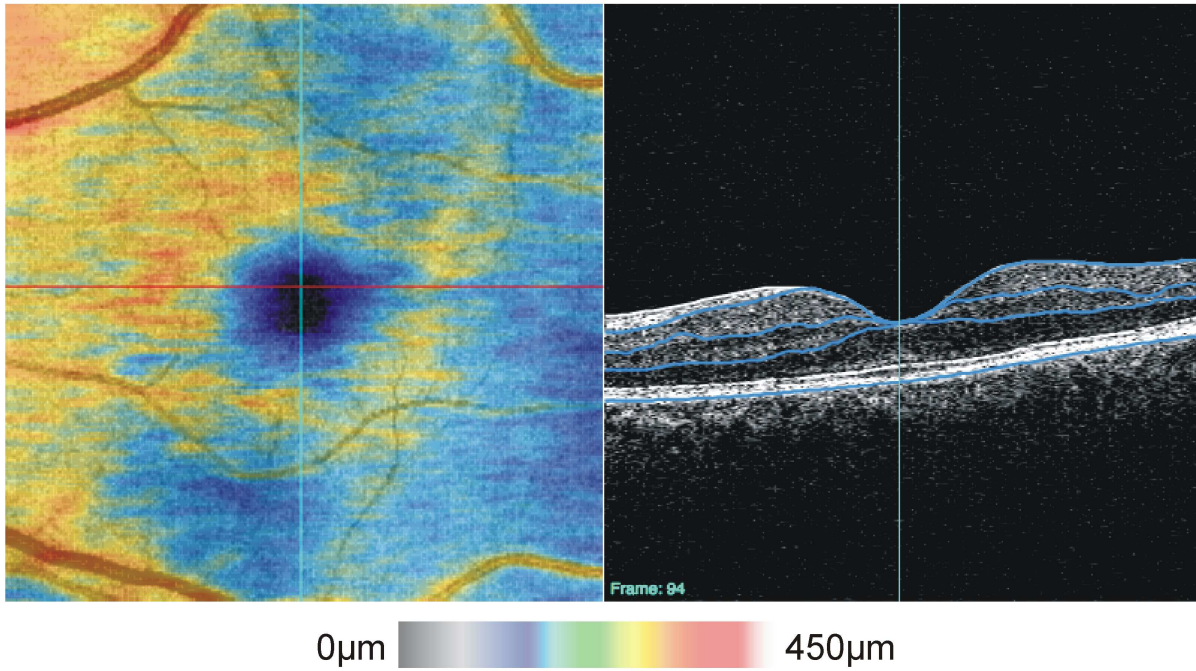
2

3 **Figure 1** (Top) OCT fundus images and (Bottom) RNFL thickness maps obtained by segmenting
4 RNFL at all locations outside of the optic nerve, for a healthy and glaucoma subject. The outer
5 red circle indicates the location of a resampled 3.4mm peripapillary cross-section. Images
6 acquired with Cirrus HD-OCT; 200x200 A-scans, 6x6 mm).
7

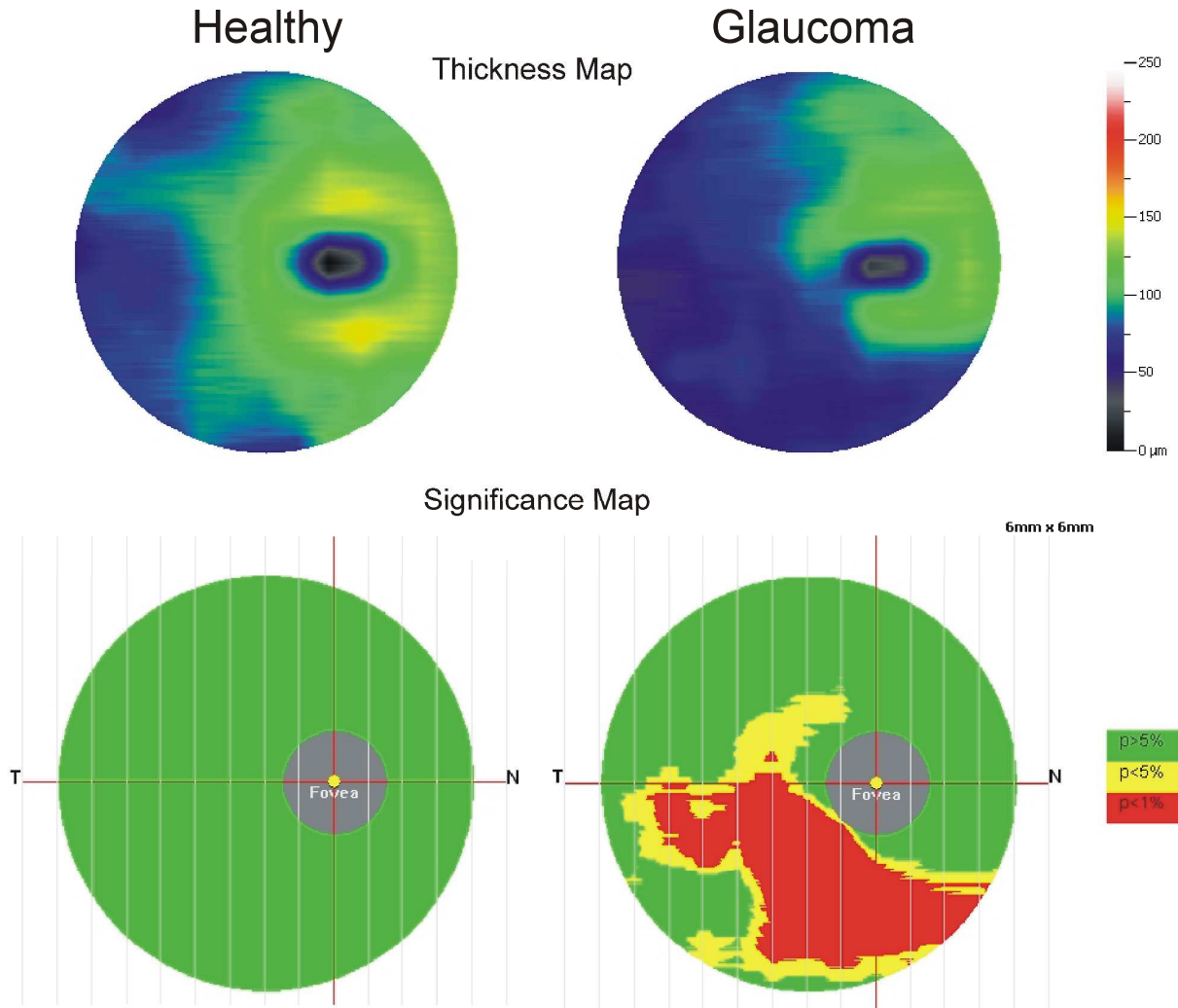


8

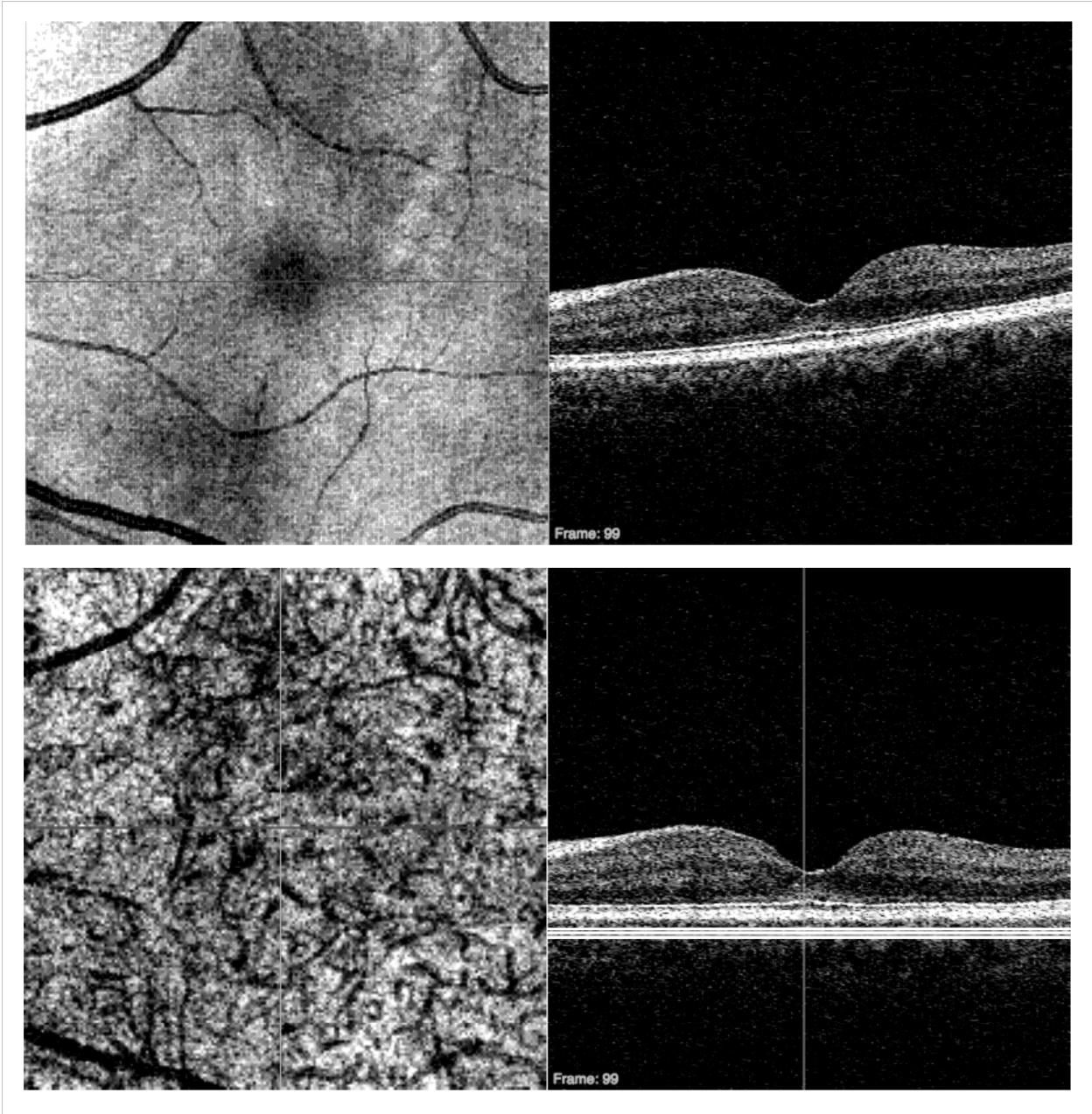
- 1 **Figure 2.** (Left) SD-OCT macular thickness map (inner retinal complex) and (Right) cross-
2 sectional image showing automated segmentation results for one frame of the 3D volume. Image
3 acquired with Cirrus HD-OCT; 200x200 A-scans, 6x6 mm); Blue lines, from inner to outer
4 retina, indicate the outer border of the retinal nerve fiber layer, outer border of the inner
5 plexiform layer, outer border of the outer plexiform layer and RPE
6



1 **Figure 3.** Ganglion cell complex thickness and significance maps for a healthy (left) and
 2 glaucoma (right) subject. The ganglion cell complex includes cell bodies, axons and dendrites of
 3 retinal ganglion cells. Images acquired with RTVue-100: 1 horizontal B-scan, and 15 vertical B-
 4 scans (separated by 0.5 mm). All B-scans consisted of 933 A-scans; 7 x 6 mm scan area).
 5



1 **Figure 4.** (Top left) Macular SD-OCT fundus image and (top right) cross section through the
2 fovea. (Bottom left) C-mode of choroidal vessels, (bottom right) based on a slab of thickness
3 indicated by the three horizontal white lines after aligning to the RPE. Image acquired with
4 Cirrus HD-OCT; 200x200 A-scans, 6x6 mm).
5



6

Table 1. Comparison of time-domain (TD-), spectral-domain (SD-) and swept-source (SS-) optical coherence tomography (OCT) devices

	Light source	Ophthalmic system commercially available?	Primary Advantages	Primary Disadvantages
TD-OCT	Broadbandwidth	Yes	Intensity information acquired in time domain; No complex conjugate image	Moving reference mirror required limiting acquisition rate
SD-OCT	Broadbandwidth	Yes	No moving reference mirror required; Higher sensitivity than TD-OCT; High scanning speed and axial resolution have been attained	Noticeable signal drop-off with depth
SS-OCT	Narrow band, swept through broad range	No	No moving reference mirror required; Higher sensitivity than TD-OCT; Very high scanning speeds can be attained; Minimal signal drop-off with depth	Most ophthalmic systems operating at longer wavelengths ($\lambda=1-1.3 \mu\text{m}$), with lower axial resolution

Table 2. Description of commercially available SD-OCT systems

Device (Manufacturer)	Description
3D-OCT 2000 (Topcon)	SD-OCT and high-resolution fundus camera; Axial resolution 5 μm , A-scan acquisition rate: 27 kHz.
Bioptigen SD-OCT (Bioptigen)	Designed for both clinical and research use and includes a hand-held probe and microscope setup; Axial resolution 4 μm , A-scan acquisition rate: 20 kHz

Cirrus HD-OCT (Carl Zeiss Meditec)	Software includes guided progression analysis for glaucoma progression detection; Axial resolution 5 μm , A-scan acquisition rate: 27 kHz.
RTVue-100 (Optovue)	Offers multiple scanning protocols for glaucoma detection, including ganglion cell complex analysis; Axial resolution 5 μm , A-scan acquisition rate: 26 kHz.
SOCT Copernicus (Optopol)	Software includes progression analysis software that incorporates disk damage likelihood scale, asymmetry between the discs, and RNFL thickness; Axial resolution 6 μm , A-scan acquisition rate: 27 kHz.
Spectral OCT SLO (Opko)	Combines SD-OCT, scanning laser ophthalmoscopy, and microperimetry. Axial resolution 6 μm , A-scan acquisition rate: 27 kHz.
Spectralis OCT (Heidelberg Engineering)	High-speed SD-OCT device with eye-tracking, fluorescein angiography, ICG angiography, and autofluorescence. Axial resolution 7 μm , A-scan acquisition rate: 40 kHz.

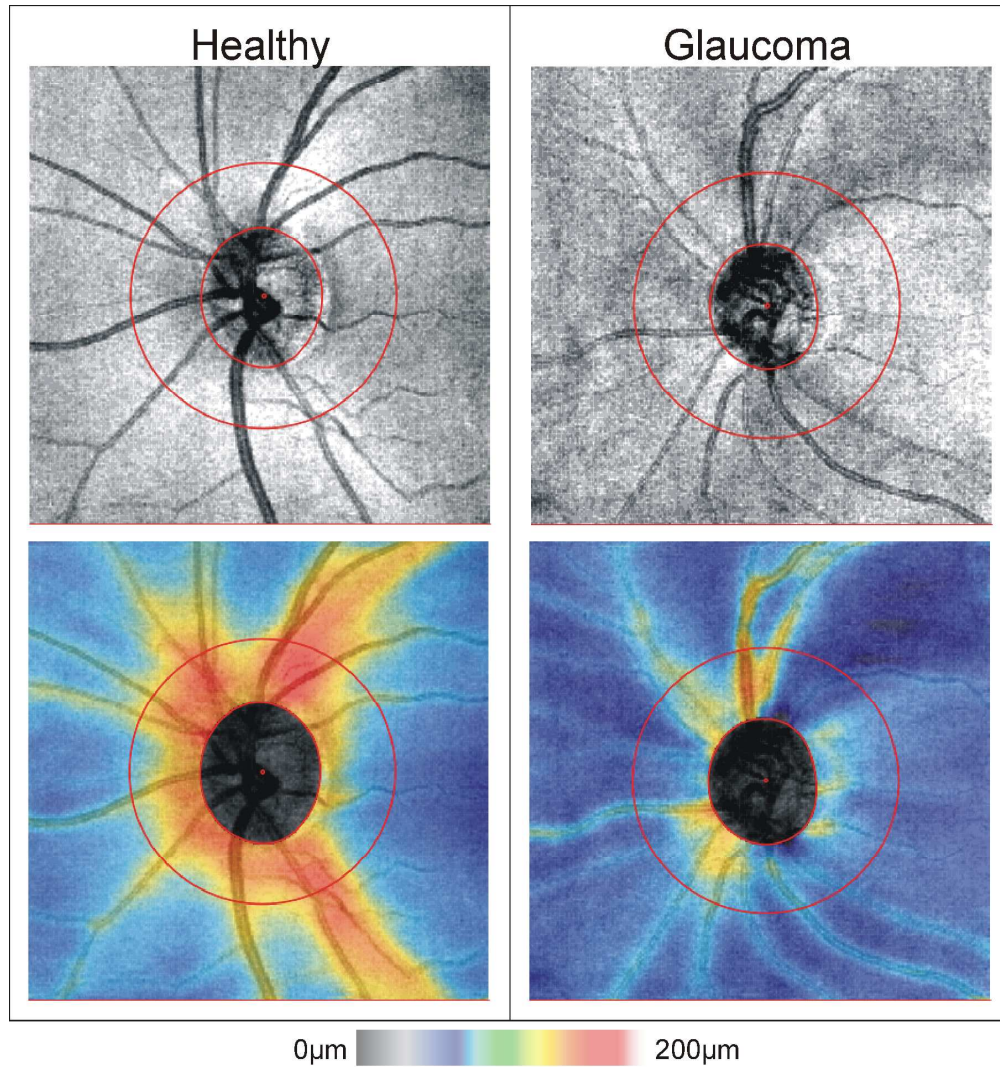


Figure 1 (Top) OCT fundus images and (Bottom) RNFL thickness maps obtained by segmenting RNFL at all locations outside of the optic nerve, for a healthy and glaucoma subject. The outer red circle indicates the location of a resampled 3.4mm peripapillary cross-section. Images acquired with Cirrus HD-OCT; 200x200 A-scans, 6x6 mm).

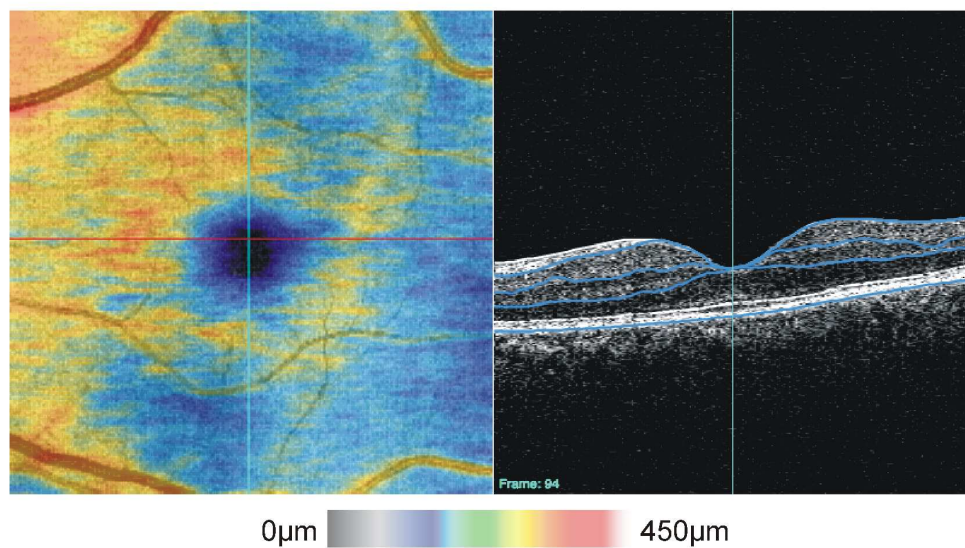


Figure 2. (Left) SD-OCT macular thickness map (inner retinal complex) and (Right) cross-sectional image showing automated segmentation results for one frame of the 3D volume. Image acquired with Cirrus HD-OCT; 200x200 A-scans, 6x6 mm); Blue lines, from inner to outer retina, indicate the outer border of the retinal nerve fiber layer, outer border of the inner plexiform layer, outer border of the outer plexiform layer and RPE

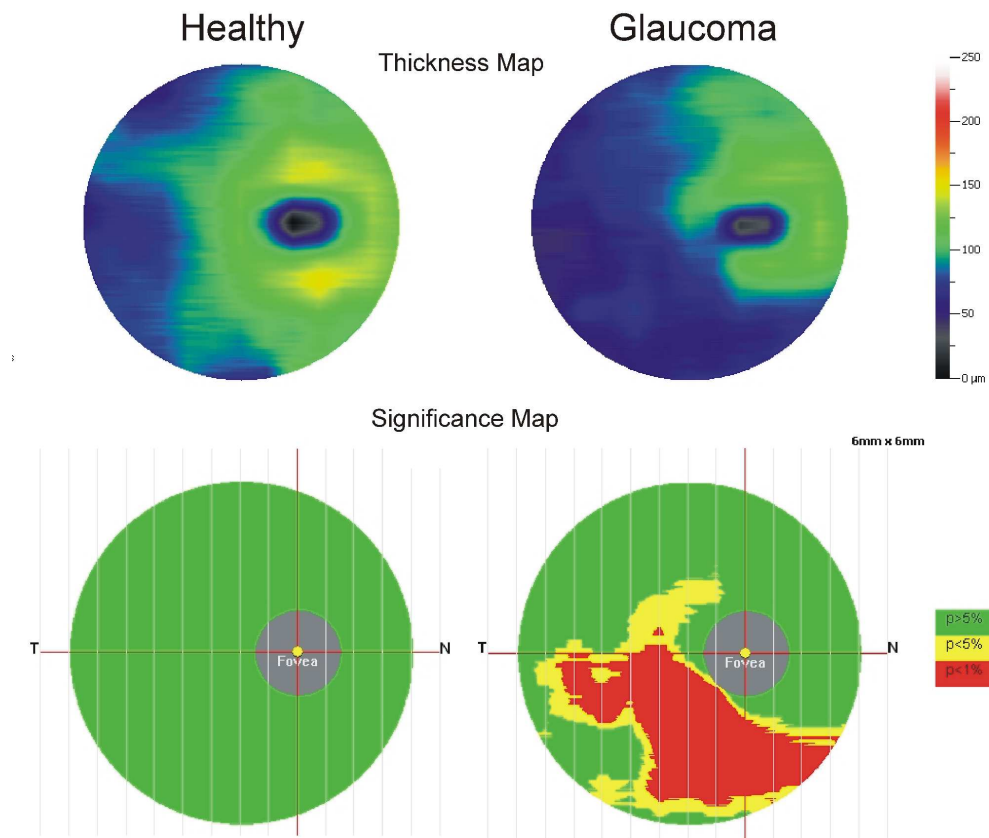


Figure 3. Ganglion cell complex thickness and significance maps for a healthy (left) and glaucoma (right) subject. The ganglion cell complex includes cell bodies, axons and dendrites of retinal ganglion cells. Images acquired with RTVue-100: 1 horizontal B-scan, and 15 vertical B-scans (separated by 0.5 mm). All B-scans consisted of 933 A-scans; 7 x 6 mm scan area).

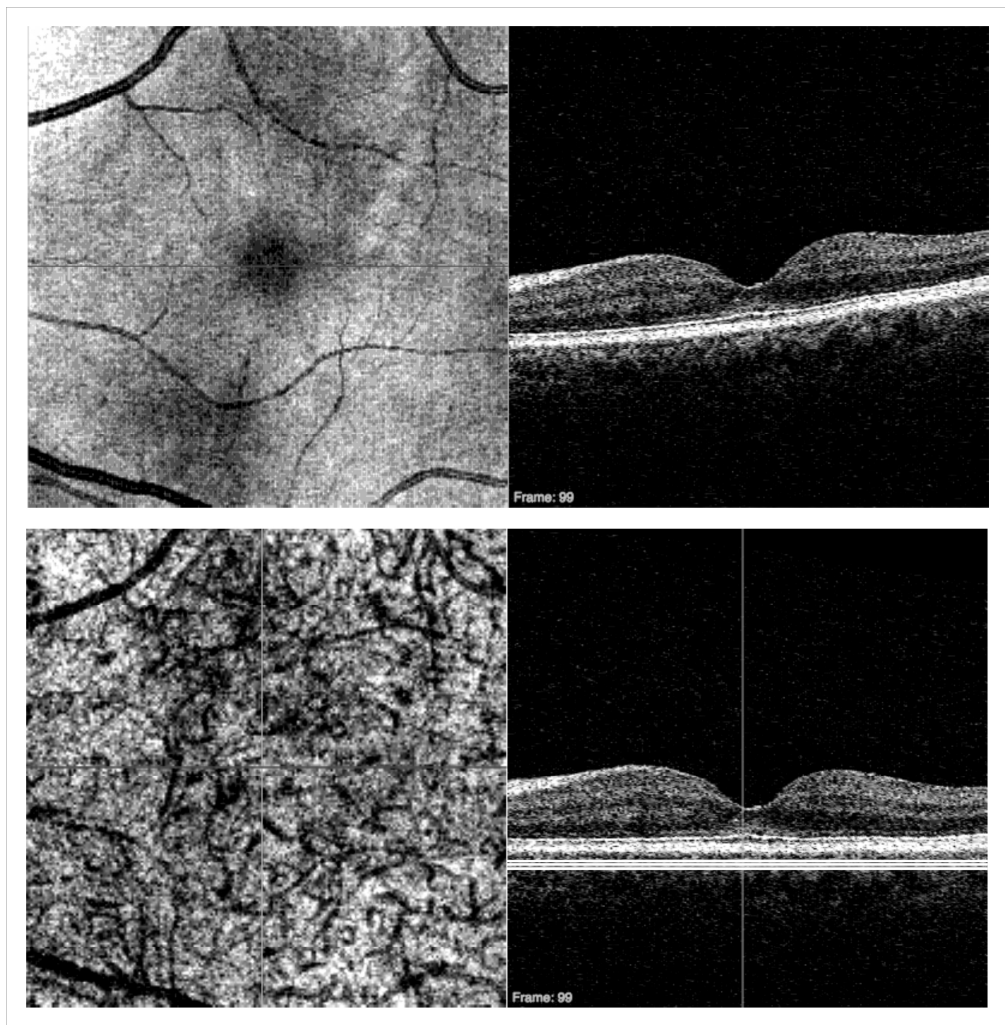


Figure 4. (Top left) Macular SD-OCT fundus image and (top right) cross section through the fovea. (Bottom left) C-mode of choroidal vessels, (bottom right) based on a slab of thickness indicated by the three horizontal white lines after aligning to the RPE. Image acquired with Cirrus HD-OCT; 200x200 A-scans, 6x6 mm).